Crystal Structure and Stability in Aqueous Solutions of $Na_{0.5}[NpO_2(OH)_{1.5}]\cdot 0.5H_2O$ and $Na[NpO_2(OH)_2]$

David Fellhauer,* Jun-Yeop Lee, Nicole A. DiBlasi, Olaf Walter, Xavier Gaona, Dieter Schild, and Marcus Altmaier

ABSTRACT: The ternary neptunium(V) (Np(V)) hydroxides $Na_{0.5}[NpO_2(OH)_{1.5}]\cdot 0.5H_2O$ (**I**) and $Na[NpO_2(OH)_2]$ (**II**) were synthesized in aqueous NaOH solutions at T = 80 °C, and their crystal structures were determined to be monoclinic, $P2_1$, Z = 2, a = 5.9859(2), b = 10.1932(3), c = 12.1524(4) Å, β = 98.864(1)°, V = 732.63(4) Å^3 for (**I**) and orthorhombic, $P2_12_12_1$, Z = 4, a = 5.856(7), b = 7.621(9), c = 8.174(9) Å, V = 364.8(7) Å^3 for (**II**). By combining the detailed structural information with results from systematic solubility investigations, a comprehensive chemical and thermodynamic model of the Np(V) behavior in NaCl−NaOH solutions was evaluated. The results reveal a great stability of the ternary Na−Np(V)−OH solid phases that significantly enhances the predominance field of the entire Np(V) redox state to high alkalinity.

Oxides and hydroxides of actinide elements (An) that form in aqueous solution are fundamental compounds from the viewpoint of environmental implications, nuclear waste disposal, and basic actinide research.[1−5] The most relevant oxidation states of early An are +III to +VI. An(V) often obtains special attention in environmental actinide studies, as it is highly mobile under various solution conditions due its low sorption behavior and high solubility.[6,7] For a detailed scientific assessment of the latter, a thorough knowledge of structure and stability of the solubility limiting An(V) solid phases is desired. The most apparent representative for studying An(V) systems is neptunium(V), as it holds the widest solution stability of all the actinides for both solid and solution species.

The number of crystal structures reported for inorganic Np(V) compounds have continuously increased within the last two decades and presently sums up to about 70.[8] Many of them contain oxo anions such as XO_3^{n-} (X = C, N, Se, I) and ZO_4^{n-} (Z = P, S, Cl, Cr, Se, Mo) or chloride as a principle structural ligand. Despite their great importance for aqueous systems, there are only five single crystal structures published for pure oxides and hydroxides of neptunium(V), namely, Np_2O_5, $Na[NpO_2(OH)_2]$, $K[NpO_2(OH)_2]\cdot 2H_2O$, $K_4[(NpO_2)_2(OH)_6]\cdot 4H_2O$, and $Rb_4[(NpO_2)_4(OH)_8]\cdot 2H_2O$.[9−12] Currently, according to their decreased stability, none have been published for Pu(V) or Am(V). Previous studies reported on the synthesis of a significantly greater number of ternary Np(V), Pu(V), and Am(V) hydroxides, e.g., $M[AnO_2(OH)_2]\cdot xH_2O$ and $M_2[AnO_2(OH)_3]\cdot xH_2O$ with M = Na−Cs for Np, M = Li, K, Rb for Pu, and M = Rb, Cs for Am, as well as $M[NpO_2(OH)_2]_2\cdot xH_2O$ and $M[NpO_2(OH)_3]\cdot xH_2O$ with M = Mg−Ba, without providing detailed structural models.[13−16] In line with the focus of these structural studies, very little information can be drawn about the solution stability of ternary M−Np(V)−OH phases and, thus, their potential environmental behavior. Recent solubility investigations performed with Np(V) hydroxides set another priority. They showed that (poly)crystalline M−Np(V)−OH solid phases (M = Na and Ca) significantly enhance the thermodynamic stability of Np(V) in alkaline NaCl and $CaCl_2$ solutions but lacked detailed structural models of the solubility controlling solid phases.[17−19] Herein, we report on the successful combination of a comprehensive structural and thermodynamic investigation of two different Na−Np(V)−OH solid phases. Synthesis,[20] crystal structures, and the results of systematic solubility studies of the hitherto unknown $Na_{0.5}[NpO_2(OH)_{1.5}]\cdot 0.5H_2O$ (**I**) and the previously reported $Na[NpO_2(OH)_2]$ (**II**) are discussed. From the thermodynamic constants derived, an updated Pourbaix diagram for aqueous neptunium systems is calculated, clearly demonstrating the high relevance of these ternary Na−Np(V)−OH regarding Np(V) stability in alkaline solutions.

Compound (**I**) crystallizes in the monoclinic space group $P2_1$ with the overall sum formula of $Na_2[NpO_2(OH)_{1.5}]_4\cdot 2H_2O$ for the crystallographic independent unit of the elementary cell and adopts a complex three dimensional framework consisting of neptunyl(V) pentagonal bipyramids; see Figure 1. The structure of (**I**) contains four distinct neptunium sites, with Np(1) ≈ Np(4) and Np(2) ≈ Np(3) showing practically the same coordination environments and very similar crystallographic features. In Np(1) and Np(4), one of the neptunyl oxygens is only coordinated to Na^+ ions with bond lengths of 1.859(5)−1.864(5) Å, whereas the second yl oxygen is a bridging ligand bonded to another Np(V) site in an

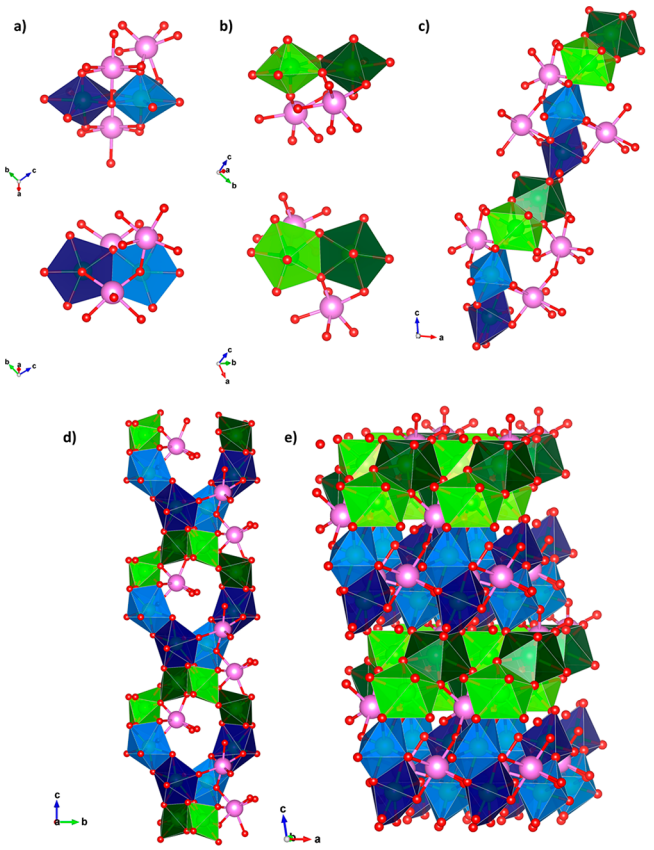

Figure 1. Solid state structure of $Na_{0.5}[NpO_2(OH)_{1.5}]\cdot 0.5H_2O$ (I).[21] Np(1)−Np(4) (a) and Np(2)−Np(3) (b) dimer building blocks, top and side view. (c) Chain composed of $\{[Np(1)-Np(4)]-[Np(2)-Np(3)]\}_n$ dimer polymerization along the 101 plane. Full structure looking into the *a* axis (d) and *c* axis (e) (Na, pink; Np(1), dark blue; Np(2), light green; Np(3), dark green; Np(4), light blue; O, red).

equatorial position (two center cation−cation interaction, CCI) with bond lengths of 1.881(5)−1.893(5) Å. The O=Np=O bond angles are 176.2(2) and 175.2(2)°, respectively. Np(1) and Np(4) are coordinated in the equatorial plane by three OH ligands (two two center bridging ligands with bond lengths of 2.346(5)−2.406(4) Å and one three center bridging ligand with bond lengths of 2.494(4)−2.512(4) Å) and two oxygen ligands from other neptunyl sites (two center CCI) with bond lengths of 2.445(4)−2.543(4) Å resulting in $(NpO_2)(O)_2(OH)_3$ pentagonal bipyramids. In Np(2) and Np(3), both neptunyl oxygens are also bridging ligands forming two center CCIs to other Np(V) sites with bond lengths ranging from 1.881(4)−1.892(4) Å and O=Np=O angles of 171.5(2) and 171.1(2)°, respectively. Np(2) and Np(3) are coordinated in the equatorial plane by four OH ligands (two two center bridging ligands with bond lengths of 2.389(5)−2.401(4) Å and two three center bridging ligands with bond lengths of 2.389(5)−2.444(4) Å) and one neptunyl oxo ligand (two center CCI) with bond lengths of 2.527(5)−2.543(5) Å resulting in $(NpO_2)O(OH)_4$ pentagonal bipyramids. The two distinct sodium sites in **(I)** are coordinated by six oxygen atoms in a distorted octahedral environment with bond lengths ranging from 2.321(6)−2.641(6) Å. Na(1) shares four oxygen atoms with neptunium polyhedra (2.417(5)−2.495(5) Å), while the other two show coordination to only the sodium atom (2.321(6) and 2.459(5) Å). Na(2) is fully coordinated to O atoms of neptunium polyhedra (2.376(5)−2.641(6) Å).

A clear pattern to describe the topology of this complex, three dimensional network of neptunyl bipyramids arises in the form of characteristic dimeric building blocks. The first dimer is constructed from Np(1) and Np(4) pentagonal bipyramids sharing an equatorial edge defined by two OH ligands (Figure 1a); the second dimer is fashioned similarly from Np(2) and Np(3) (Figure 1b). Adjacent pairs of Np(1)−Np(4) and Np(2)−Np(3) dimers share single equatorial vertices to form chains of the type $\{[Np(1)-Np(4)]-[Np(2)-Np(3)]\}_n$, in which each dimer is connected to the next through a CCI interaction; Np(4) shares an equatorial edge with an yl and equatorial oxygen from Np(2), while Np(3) shares the *trans* yl oxygen (compared to Np(2)) and an equatorial oxygen with an equatorial edge of Np(1) (Figure 1c). This chain propagates diagonally along the *a*−*c* plane, and each dimer is situated diagonally within the *b*−*c* plane, resulting in a corrugated chain that returns to the same *b* position with each repetition. The chains are then cross linked through additional CCIs between Np(2)−Np(3) dimers along the *b* axis, a corner sharing CCI between Np(1)−Np(4) dimers, which involves a single Np(1) yl oxygen also behaving as an Np(4) equatorial oxygen, and bridging Na(2) coordination. The resulting framework of **(I)** contains large channels extending along the *a* axis, in which Na(1) atoms and interstitial water molecules reside (Figure 1d).

The structure of orthorhombic $Na[NpO_2(OH)_2]$ **(II)** was first reported by Almond et al.[10] The crystallographic information for **(II)** discussed in the following are based on the independent single crystal analysis performed within the present work. It fits well to the data of Almond et al., whose results are given in curly brackets for comparison. **(II)** contains one crystallographically unique NpO_2^+ ion with Np=O bond lengths of 1.866(19)−1.871(18) {1.879(3)−1.895(3)} Å and an O=Np=O bond angle of 177.1(12)° {179.6(1)°}. It is coordinated in the equatorial plane by four OH ligands with bond lengths ranging from 2.38(3)−2.45(3) {2.377(3)−2.437(3)} Å and one neptunyl oxo ligand (two center CCI) with a bond length of 2.48(2) {2.470(3)} Å from an adjacent neptunium site. In **(II)**, the $(NpO_2)O(OH)_4$ pentagonal bipyramids share equatorial edges defined by hydroxyl ligands, forming chains that extend along the *b* axis; see Figure 2. The chains are linked through two center CCIs (end on) into a three dimensional network. **(II)** contains one unique sodium site that is located in channels extending along the *b* axis.

To gain insight into their thermodynamic stability, the solubility behavior of both solid phases was investigated in 1.02 $mol\cdot kg^{-1}(H_2O)$ NaCl−NaOH solutions as a function of pH_m = 8.5−13. Figure 3a shows the experimental solubility curves of **(I)** and **(II)** as plots of log $m_{Np(V)}$ versus $pH_m = -\log m_{H+}$, in comparison to conditional model calculations.

Compared to the most fundamental Np(V) hydroxide compound, binary $NpO_2OH(am)$, **(I)** and **(II)** are signifi cantly less soluble and, thus, exhibit a greater stability under the given experimental conditions. This highlights that $NpO_2OH(am)$ is only metastable in alkaline sodium containing solutions. As indicated by the intersecting solubility curves of **(I)** and **(II)** in Figure 3a, **(I)** is thermodynamically more stable at $pH_m \leq 10.6$, and **(II)** is more stable at $pH_m > 10.6$. For both Na−Np(V)−OH solids, measured Np(V) equilibrium concentrations systematically decrease with increasing pH_m up to $pH_m \approx 10.5$, showing slopes of $m \approx$

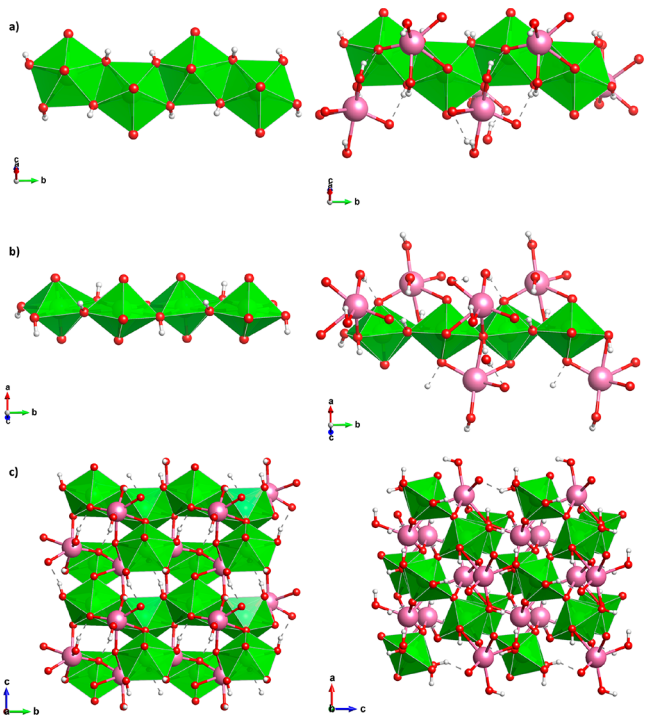

Figure 2. Solid state structure of $Na[NpO_2(OH)_2]$ (**II**).[21] (NpO_2)$O(OH)_4$ pentagonal bipyramid chain along the *b* axis with and without Na from the (a) top view or (b) side view, and (c) full structure looking into the *a* axis to highlight the CCI and *b* axis to highlight the Na placement in structural channels (Na, pink; Np, light green; O, red; H, white).

-1.5 ± 0.1 for (**I**) and $m \approx -1.7 \pm 0.2$ for (**II**). Above $pH_m \approx 10.5$, the solubility curves first start to flatten and then pass a minimum at about $pH_m \approx 11.9$ for (**I**) with $\log [Np(V)]_{min} = -7.4 \pm 0.1$ and $pH_m \approx 12.2$ for (**II**) with $\log [Np(V)]_{min} = -8.0 \pm 0.1$ and finally increase again.

The observed behavior, including the apparent differences between both systems, can be understood by considering the different hydroxide contents in (**I**) and (**II**) and the dependence of the aqueous Np(V) speciation on pH_m. Based on the critical review by the NEA TDB project, the $NpO_2^+(aq)$ aquo ion is the main species up to $pH_m \approx 11.3$, the first hydrolysis species $NpO_2(OH)(aq)$ becomes predominant within the range $\sim 11.3 < pH_m < \sim 12$, and the second hydrolysis complex $NpO_2(OH)_2^-$ predominates above $pH_m \approx 12$.[2] Other studies further propose the presence of a third hydrolysis complex at greater alkalinity.[22,23] Therefore, the following reactions can be considered to control the Np(V) solubility in equilibrium with compounds (**I**) and (**II**) as a function of pH_m

$$Na_{0.5}[NpO_2(OH)_{1.5}]\cdot 0.5H_2O(\mathbf{I}) + (1.5 - n)H^+ \Leftrightarrow 0.5Na^+ + NpO_2(OH)_n^{1-n} + (2 - n)H_2O$$

and

$$Na[NpO_2(OH)_2](\mathbf{II}) + (2 - n)H^+ \Leftrightarrow Na^+ + NpO_2(OH)_n^{1-n} + (2 - n)H_2O,$$

with $n = 0$–3

By using these reactions as the basic chemical model, solubility constants $\log {}^*K'_{s,0}$ for (**I**) and (**II**) and hydrolysis constants

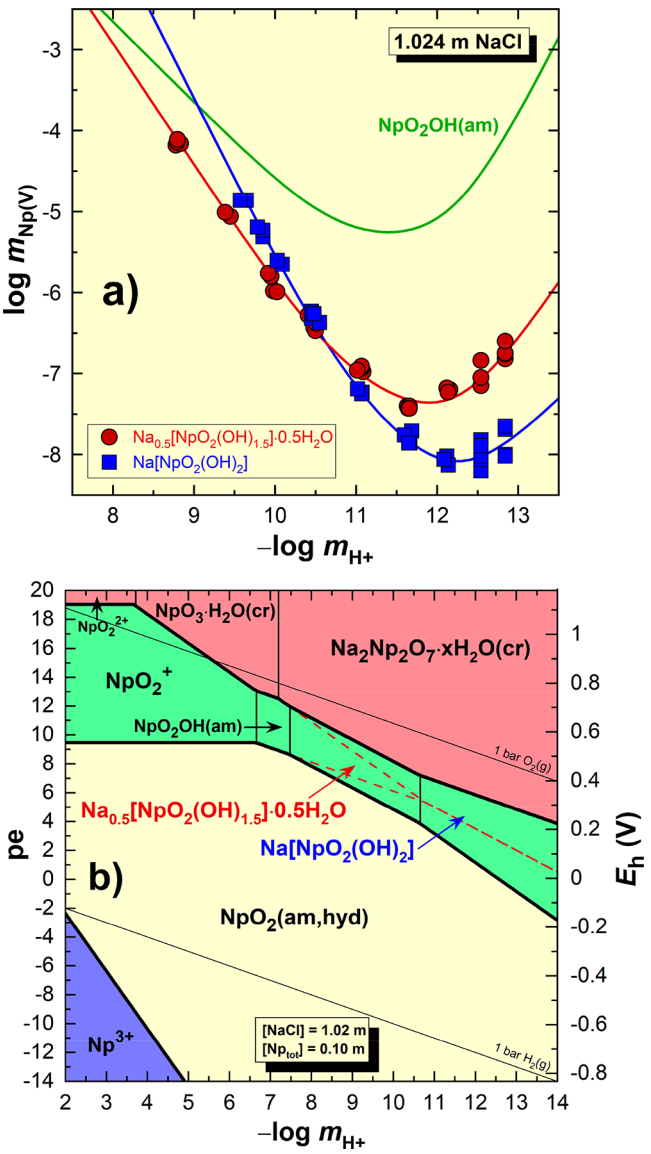

Figure 3. (a) Experimental and modeled molal Np(V) solubility, $m_{Np(V)}$, of $Na_{0.5}[NpO_2(OH)_{1.5}]\cdot 0.5H_2O$ (**I**), $Na[NpO_2(OH)_2]$ (**II**), and $NpO_2OH(am)$ in 1.02 $mol\cdot kg^{-1}(H_2O)$ NaCl solution. (b) Pourbaix diagram for neptunium in 1.02 $mol\cdot kg^{-1}(H_2O)$ NaCl solution. Calculations in (a) and (b) were performed with thermodynamic data reported in NEA TDB extended by the constants derived in this work.[2] The stability fields indicated by the dashed lines in graph (b) neglect the formation of the new Na–Np(V)–OH phases.

$\log {}^*\beta'_n$ with $n = 1$, 2, and 3 were fitted from the experimental data with the model code *fiteql*; see Table 1.[24]

Our results suggest slightly greater formation constants for the first and second hydrolysis complexes of Np(V) compared to the values recommended by NEA TDB. Additionally, our results clearly confirm contributions from the third hydrolysis species, $NpO_2(OH)_3^{2-}$, which becomes predominant at $pH_m \geq 12.3$. The fact that very consistent $\log {}^*\beta'_n$ values are obtained from the independent solubility data for (**I**) and (**II**) and that well defined Np(V) hydroxides were used in the present study corroborate a high reliability of our evaluated constants. In contrast, $\log {}^*\beta'_n$ constants recommended by the NEA TDB were derived from experimental solubility studies performed with an uncharacterized Np(V) solid phase considered to be

Table 1. Conditional Hydrolysis and Solubility Constants Valid for 1.02 mol·kg^{-1}(H_2O) NaCl Evaluated from the Solubility Data for Compounds (I) and (II) in Comparison to the Values Reported by NEA TDB[a]

	log $*\beta'_1$	log $*\beta'_2$	log $*\beta'_3$	log $*K'_{s,0}$
(I)	10.82 ± 0.09	22.85 ± 0.16	35.18 ± 0.10	9.08 ± 0.03
(II)	10.70 ± 0.11	22.93 ± 0.17	35.27 ± 0.11	14.40 ± 0.03
NEA	11.3 ± 0.7	23.3 ± 0.5	n.a.	n.a.

[a]All uncertainties correspond to the 2σ confidence level.

$NpO_2OH(am)$. This fact gave cause to some debates as recently summarized in Petrov et al. and is reflected by the large uncertainty values of the current NEA TDB data.[19]

The current NEA TDB database provides recommended solubility constants for only one Np(V) hydroxide compound that is relevant for the H−Na−Cl−OH−H_2O system: $NpO_2OH(am)$. Due to the great thermodynamic stability of the redox neighbors Np(IV) and Np(VI), the modeled predominance field of $NpO_2OH(am)$ and, hence, of solid Np(V) ends at about $pH_m \approx 11$ as indicated by the red dotted line in Figure 3b. When including the new constants for **(I)** and **(II)** in the calculation of an updated neptunium Pourbaix diagram, the picture changes significantly. As a function of increasing pH_m, the stability of $NpO_2OH(am)$ now ends at $pH_m \approx 7.5$, and new substantial stability fields evolve for compound **(I)** up to $pH_m \approx 10.6$ and **(II)** at $pH_m > \sim 10.6$. This results in an overall stability field for pentavalent neptunium in NaCl−NaOH solution extending up to a pH_m of 14 that can, for the first time, be verified in terms of equilibrium thermodynamics.

These present results, which report a new crystal structure for a Np(V)−OH solid phase, confirm the structure for a second, and generate an updated thermochemical model for neptunium hydroxide stability, significantly improve the understanding of actinide solution and structural chemistry on a quantitative basis with potential implications for environmental and nuclear waste disposal applications.

■ ASSOCIATED CONTENT

● Supporting Information

The Supporting Information is available free of charge at https://pubs.acs.org/doi/10.1021/jacs.2c03479.

> Additional depictions of the structures for $Na_{0.5}[NpO_2(OH)_{1.5}]\cdot 0.5H_2O$ (I) and $Na[NpO_2(OH)_2]$ (II), additional experimental details and methods, additional information on thermodynamic evaluation, tables with solubility data (PDF)

Accession Codes

CCDC 2160534−2160535 contain the supplementary crystallographic data for this paper. These data can be obtained free of charge via www.ccdc.cam.ac.uk/data request/cif, or by emailing data request@ccdc.cam.ac.uk

■ AUTHOR INFORMATION

Corresponding Author

David Fellhauer − *Institute for Nuclear Waste Disposal, Karlsruhe Institute of Technology, 76021 Karlsruhe, Germany;* orcid.org/0000 0002 7440 0790; Email: david.fellhauer@kit.edu

Authors

Jun Yeop Lee − *School of Mechanical Engineering, Pusan National University, Geumjeong gu, Busan 46241, South Korea;* orcid.org/0000 0001 5348 9629

Nicole A. DiBlasi − *Institute for Nuclear Waste Disposal, Karlsruhe Institute of Technology, 76021 Karlsruhe, Germany;* orcid.org/0000 0003 4385 0438

Olaf Walter − *Joint Research Centre Karlsruhe, European Commission, 76125 Karlsruhe, Germany;* orcid.org/0000 0002 2679 1715

Xavier Gaona − *Institute for Nuclear Waste Disposal, Karlsruhe Institute of Technology, 76021 Karlsruhe, Germany*

Dieter Schild − *Institute for Nuclear Waste Disposal, Karlsruhe Institute of Technology, 76021 Karlsruhe, Germany;* orcid.org/0000 0001 6034 8146

Marcus Altmaier − *Institute for Nuclear Waste Disposal, Karlsruhe Institute of Technology, 76021 Karlsruhe, Germany*

Notes

The authors declare no competing financial interest.

■ ACKNOWLEDGMENTS

This work was supported by the German Federal Ministry of Education and Research under contract 02NUK039A, the ThermAc project.

■ REFERENCES

(1) Silva, R. J.; Nitsche, H. Actinide Environmental Chemistry. *Radiochim. Acta* **1995**, *70 71*, 377−396.

(2) Grenthe, I.; Gaona, X.; Plyasunov, A. V.; Rao, L.; Runde, W. H.; Grambow, B.; Konings, R. J. M.; Smith, A. L.; Moore, E. E. *Second Update on the Chemical Thermodynamics of Uranium, Neptunium, Plutonium, Americium and Technetium*; OECD Publications: Paris, France, 2020.

(3) Wanner, H. Solubility Data in Radioactive Waste Disposal. *Pure Appl. Chem.* **2007**, *79*, 875−882.

(4) Qiu, J.; Burns, P. C. Clusters of Actinides with Oxide, Peroxide, or Hydroxide Bridges. *Chem. Rev.* **2013**, *113*, 1097−1120.

(5) Knope, K. E.; Soderholm, L. Solution and Solid State Structural Chemistry of Actinide Hydrates and Their Hydrolysis and Condensation Products. *Chem. Rev.* **2013**, *113*, 944−994.

(6) Choppin, G. R. Solution Chemistry of the Actinides. *Radiochim. Acta* **1983**, *32*, 43−53.

(7) Maher, K.; Bargar, J. R.; Brown, G. E. Jr. Environmental Speciation of Actinides. *Inorg. Chem.* **2013**, *52*, 3510−3532.

(8) Gilson, S. E.; Burns, P. C. The Crystal and Coordination Chemistry of Neptunium in all its Oxidation States: An Expanded Structural Hierarchy of Neptunium Compounds. *Coord. Chem. Rev.* **2021**, *445*, 213994.

(9) Forbes, T. Z.; Burns, P. C.; Skanthakumar, S.; Soderholm, L. Synthesis, Structure, and Magnetism of Np_2O_5. *J. Am. Chem. Soc.* **2007**, *129*, 2760−2761.

(10) Almond, P. M.; Skanthakumar, S.; Soderholm, L.; Burns, P. C. Cation Cation Interactions and Antiferromagnetism in $Na[Np(V)O_2(OH)_2]$: Synthesis, Structure, and Magnetic Properties. *Chem. Mater.* **2007**, *19*, 280−285.
(11) Vlaisavljevich, B.; Miró, P.; Ma, D.; Sigmon, G. E.; Burns, P. C.; Cramer, C. J.; Gagliardi, L. Synthesis and Characterization of the First 2D Neptunyl Structure Stabilized by Side on Cation Cation Interactions. *Chem. Eur. J.* **2013**, *19*, 2937−2941.
(12) Wilson, R. E.; Stegman, S.; Tarlton, M. L. Reactions of Neptunium(V) in Alkali Metal Hydroxides. *Inorg. Chem.* **2021**, *60*, 17480−17486.
(13) Visyachscheva, G. I.; Volkov, Y. F.; Simakin, G. A.; Kapshukov, G. I. Some Hydroxides of Pentavalent Neptunium. *Sov. Radiochem.* **1984**, *26*, 156−160.
(14) Tananaev, I. G. Solid state Reaction of Certain Neptunium(V) Compounds with Bases. *Sov. Radiochem.* **1991**, *33*, 219−223.
(15) Tananaev, I. G. New Np(V) Hydroxide Compounds. *Sov. Radiochem.* **1991**, *33*, 652−656.
(16) Tananaev, I. G. New Hydroxide Compounds of Np(V). *Sov. Radiochem.* **1992**, *34*, 85−89.
(17) Fellhauer, D.; Rothe, J.; Altmaier, M.; Neck, V.; Runke, J.; Wiss, T.; Fanghänel, Th. Np(V) Solubility, Speciation and Solid Phase Formation in Alkaline $CaCl_2$ Solutions. Part I: Experimental Results. *Radiochim. Acta* **2016**, *104*, 355−379.
(18) Fellhauer, D.; Altmaier, M.; Gaona, X.; Lützenkirchen, J.; Fanghänel, Th. Np(V) Solubility, Speciation and Solid Phase Formation in Alkaline $CaCl_2$ Solutions. Part II: Thermodynamics and Implications for Source Term Estimations of Nuclear Waste Disposal. *Radiochim. Acta* **2016**, *104*, 381−397.
(19) Petrov, V. G.; Fellhauer, D.; Gaona, X.; Dardenne, K.; Rothe, J.; Kalmykov, S. N.; Altmaier, M. Solubility and Hydrolysis of Np(V) in Dilute to Concentrated Alkaline NaCl Solutions: Formation of Na Np(V) OH Solid Phases at 22 °C. *Radiochim. Acta* **2017**, *105*, 1−20.
(20) $Na_{0.5}[NpO_2(OH)_{1.5}]\cdot 0.5H_2O$ (**I**) was synthesized by adding 3.0 mL of $15\cdot 10^{-3}$ mol·L^{-1} of NpO_2^+ in 0.25 mol·L^{-1} of HCl to a 50 mL screw capped PTFE vessel containing 33 mL of 0.1 mol·L^{-1} of NaOH and equilibrating the resulting initial suspension at T = 80 °C for 32 days. $Na[NpO_2(OH)_2]$ (**II**) was synthesized by adding 3.0 mL of $15\cdot 10^{-3}$ mol·L^{-1} of NpO_2^+ in 0.25 mol·L^{-1} of HCl to a 50 mL screw capped PTFE vessel containing 33 mL of 1.0 mol·L^{-1} of NaOH and equilibrating the resulting initial suspension at T = 80 °C for 32 days. Details are described in the Supporting Information.
(21) Drawings produced with VESTA: Momma, K.; Izumi, F. VESTA 3 for Three Dimensional Visualization of Crystal, Volumetric and Morphology Data. *J. Appl. Crystallogr.* **2011**, *44*, 1272−1276.
(22) Tananaev, I. G. Forms of Np(V) and Am(V) in Basic Aqueous Media. *Sov. Radiochem.* **1990**, *32*, 476−479.
(23) Shilov, V. P.; Gogolev, A. V.; Fedoseev, A. M. Speciation, Stability, and Reactions of Np(III VII) in Aqueous Solutions. *Radiochemistry* **2012**, *54*, 212−227.
(24) Herbelin, A. L.; Westall, J. C. *FITEQL, a Computer Program for Determination of Chemical Equilibrium Constants from Experimental Data*; Version 4.0, Report 99−01; Department of Chemistry, Oregon State University: Corvallis, OR, 1999.

Supporting Information

Crystal structure and stability in aqueous solutions of $Na_{0.5}[NpO_2(OH)_{1.5}]\cdot 0.5H_2O$ and $Na[NpO_2(OH)_2]$

David Fellhauer[1]*, Jun-Yeop Lee[2], Nicole A. DiBlasi[1], Olaf Walter[3], Xavier Gaona[1], Dieter Schild[1], Marcus Altmaier[1]

1 Institute for Nuclear Waste Disposal, Karlsruhe Institute of Technology, P.O. Box 3640, 76021 Karlsruhe, Germany

2 School of Mechanical Engineering, Pusan National University, 2, Busandaehak-ro 63beon-gil, Geumjeong-gu, Busan 46241, South Korea

3 Joint Research Centre Karlsruhe, European Commission, P.O. Box 2340, 76125 Karlsruhe, Germany

Corresponding Author: david.fellhauer@kit.edu

Content

1. Experimental

1.1 General

All experiments were conducted under controlled Ar atmosphere conditions in a glove box (O_2 < 5 ppm, T = 23 ± 2ºC) in the controlled area of Karlsruhe Institute of Technology – Institute for Nuclear Waste Disposal (KIT-INE). Aqueous solutions were prepared with purified, Ar-purged water (Milli-Q-academic, Millipore). Titrisol® concentrates (Merck) were used to prepare HCl and NaOH stock solutions. NaCl (p.a., Merck) was used to prepare neutral stock solutions with [NaCl] = 1.0 mol·L^{-1} (1.02 mol·kg^{-1}(H_2O)). Ion-exchange column purified and oxidation state pure $^{237}NpO_2^+$ stock solutions ($55 \cdot 10^{-3}$ mol·L^{-1} Np in 0.1 mol·L^{-1} HCl and $15 \cdot 10^{-3}$ mol·L^{-1} Np in 0.25 mol·L^{-1} HCl) from KIT-INE were used for this study. The latter were thoroughly characterized by liquid scintillation counting (LSC, Tri-Carb 3110 TR, Perkin Elmer), inductively coupled plasma-mass spectrometry (ICP-MS, Elan 6100, Perkin Elmer) and gamma spectrometry (Alpha Analyst spectrometer, Canberra), and their oxidation state were confirmed to be ≥ 98% in Np(V) by a liquid extraction technique as outlined in section 1.8. Batch solubility experiments were conducted in HD-PE vials, synthesis of the Np solid phases in PTFE vessels or PTFE-lined stainless-steel autoclave. To avoid potential interferences from fluoride traces, PTFE material were cleaned before use according to the ASTM procedure C1285-02.[1]

1.2 Synthesis of $Na_{0.5}[NpO_2(OH)_{1.5}]\cdot 0.5H_2O$ (I)

$Na_{0.5}[NpO_2(OH)_{1.5}]\cdot 0.5H_2O$ (I) was synthesized by adding 300 µL of 0.2 mol·L^{-1} NaOH to a 2 mL screw capped PP vessel (Sarstedt) containing 400 µL of the $55 \cdot 10^{-3}$ mol·L^{-1} $^{237}NpO_2^+$ stock solution in 0.1 mol·L^{-1} HCl (5.2 mg of Np) resulting in the precipitation of greenish NpO_2OH(am). The latter was separated from the mother liquor by laboratory centrifugation, washed twice with 0.01 mol·L^{-1} NaOH, and equilibrated with 20 mL of 0.1 mol·L^{-1} NaOH (corresponding to pH_m ≈12.7) in a tightly sealed PTFE-lined stainless-steel autoclave. After 30 days of tempering at T = 80 ± 5°C, the autoclave was gradually cooled down to room temperature within 96 hours. The synthesis resulted in dark-violet crystals.

In a ***second synthesis***, additional material of **$Na_{0.5}[NpO_2(OH)_{1.5}]\cdot 0.5H_2O$ (I)** used for the ***solubility study*** were successfully prepared by a very similar procedure. 3.0 mL of the $15 \cdot 10^{-3}$ mol·L^{-1} $^{237}NpO_2^+$ stock solution in 0.25 mol·L^{-1} HCl (10.7 mg of Np) were added to a screw capped PTFE vessel (50 mL, Vitlab) containing 33 mL of 0.1 mol·L^{-1} NaOH resulting in the precipitation of greenish NpO_2OH(am) and a final solution composition being [NaOH] ≈0.071 mol·L^{-1} and [NaCl] ≈0.021 mol·L^{-1} (corresponding to pH_m ≈12.5). The closed vessel containing the suspension was equilibrated at T = 80 ± 5°C. After 32 days, the material was cooled down to room temperature within three hours. The synthesis resulted in dark-violet crystals.

1.3 Synthesis of $Na[NpO_2(OH)_2]$ (II)

$Na[NpO_2(OH)_2]$ (II) was synthesized by adding 3.0 mL of the 15 mM NpO_2^+ stock solution in 0.25 M HCl (10.7 mg of Np) to a screw capped PTFE vessel (50 mL, Vitlab) containing 33 mL of 1.0 M NaOH resulting in the precipitation of greenish $NpO_2OH(am)$ and a final solution composition being [NaOH] $\approx$0.89 mol·L^{-1} and [NaCl] $\approx$0.021 mol·L^{-1} (corresponding to $pH_m \approx 13.7$). The closed vessel containing the suspension was equilibrated at $T = 80 \pm 5$°C. After 32 days, the material was cooled down to room temperature within three hours. The synthesis resulted in pinkish crystals.

1.4 Solid phase characterization

For the analysis by powder X-ray diffraction (XRD; D8 Advance, Bruker), combined scanning electron microscopy and energy-dispersive X-ray spectroscopy (SEM-EDX; FEI Quanta 650 FEG, now Thermo Fisher Scientific Inc., equipped with a UltraDry™ Peltier cooled silicon drift X-ray detector and Pathfinder software, version 2.8), solid state Vis/NIR spectroscopy (Lambda 1050+ with a 150 mm integration sphere with InGaAs detector for reflection measurements, Perkin-Elmer), and digital microscopy (VHX-1000, Keyence), a sufficient fraction (about 0.05-1.0 mg, depending on the method) of the synthesized solid phases was separated from the main vessel by centrifugation, washed 2-3 times with 1 mL of ethanol, and placed as a wet paste on the corresponding sample holder, where the material dried within few minutes inside the Ar glove box. For the quantitative analysis of structural Na and Np contents in the solid phases, about 0.5-1 mg of the washed material was digested in 1 mL of 2 % HNO_3, and the solution analyzed for Na by inductively coupled plasma optical emission spectroscopy (ICP-OES, PerkinElmer Inc., Optima 4300 DV), and for Np by liquid scintillation counting (LSC; details see section 1.7). To obtain information about the Np oxidation state distribution, fractions of approx. 0.5 mg of the washed solid phases were digested in 600 µL 1.0 mol·L^{-1} HCl and analyzed according to the solvent extraction scheme described in section 1.8. At the termination of the solubility study, solid phases retrieved from selected batch samples were analyzed again by powder XRD.

1.5 Single crystal X-ray diffraction (scx)

XRD measurements were performed on a Bruker Apex II Quazar diffractometer collecting minimum one complete full sphere of data. Frames were collected with an irradiation time of several seconds per frame appropriate to size and diffracting abilities of the crystals; a mixed ω– and φ-scan technique was employed for data collection with $\Delta\omega = \Delta\varphi = 0.5°$. Data were integrated with SAINT, corrected to Lorentz and polarisation effects and an empirical adsorption correction with SADABS was applied.[2] The structures were solved by direct methods and refined to an optimum R1 value with shelx-2013.[3] Compound (II) was best described as a twinned crystal, integration of the data performed with SAINT and absorption corrections with TWINABS.[2] For more details please see Table 2 and Table 3.

The structures have been deposited at The Cambridge Crystallographic Data Centre (CCDC) with the reference CSD numbers **2160534 (I)** and **2160535 (II)**, they contain the supplementary crystallographic data for this paper. These data can be obtained free of charge from the CCDC/CSD via https://icsd.fiz-karlsruhe.de/search/basic.xhtml.

1.6 Undersaturation solubility study

$Na_{0.5}[NpO_2(OH)_{1.5}]\cdot 0.5H_2O$ (I) obtained in the 2nd synthesis and $Na[NpO_2(OH)_2]$ (II) were used for the batch solubility study. Appropriate volumes of 1.02 $mol\cdot kg^{-1}(H_2O)$ NaCl and 1.0 $mol\cdot L^{-1}$ NaOH stock solutions were mixed to obtain NaCl-NaOH matrix solutions with ionic strength I = 1.02 $mol\cdot kg^{-1}(H_2O)$ and pH_m = 8–13. About 0.5 to 1.5 mg of the corresponding solid phase were immersed in 5 mL of these pH_m adjusted solutions in 6 mL HD-PE vials (undersaturation approach) to make nine independent samples each. 2 to 5 samplings of pH_m and [Np(V)] were performed within several weeks to months. The results are summarized in Table 7 and Table 8. The stability of the initially added solid phases (**(I)** and **(II)**, respectively) during the solubility study were confirmed by powder XRD analysis, see Figure 3 and Figure 5. The later was performed at the termination of the solubility study in four samples of each system which were selected in a way that the entire pH_m range is covered.

1.7 Determination of pH and Np concentration

The pH values in the solubility samples were determined with a combination glass electrode (Ross type, Orion) calibrated against pH standard buffer solutions (pH 6-12, Merck) before use. The experimentally measured pH values (pH_{exp}) were converted into the molal proton concentration scale ($pH_m = -\log m_{H^+}$) according to $pH_m = pH_{exp} + A_m$ with A_m = +0.08 for 1.02 $mol\cdot kg^{-1}(H_2O)$ NaCl-NaOH. Details of this approach are described in Altmaier *et al.*[4] pH measurements with glass electrodes are less reliable in hyperalkaline solutions, *e.g.*, due to the alkali error. The pH_m values of solubility samples with $pH_m \geq 12$ were therefore calculated from the analytical (initial) $[OH^-]$ in these samples according to $pH_m = \log m_{OH^-} - \log K'_w$, where $\log K'_w = -13.74$ in 1.02 $mol\cdot kg^{-1}(H_2O)$ NaCl is the conditional ionic product of water for the reaction $H_2O \Leftrightarrow H^+ + OH^-$.[5] Note, that hydroxide consuming or releasing reactions like the partial dissolution of the added Np(V) solid phases during the equilibration are negligible with respect to the great excess of $[OH^-]$ in the samples with $pH_m \geq 12$.

The Np concentration of a sample was routinely measured after a phase separation step by 10 kD ultrafiltration (10 kD ≈ 2 nm, nanosep, Pall Corporation) by liquid scintillation counting of the ^{237}Np alpha activity after *α/β* discrimination of the beta counts from the daughter ^{233}Pa on a Tri-Carb 3110 TR liquid scintillation counter (Perkin Elmer) using Ultima Gold XR cocktail (Perkin Elmer). The detection limit for ^{237}Np is approx. $1\cdot 10^{-8}$ M. In some samplings, [Np] was also determined in the clear supernatant without an ultrafiltration step. No significant differences were observed between 10kD and supernatant analysis corroborating that sorption of Np(V) on the 10kD ultrafilter is negligible under the experimental

conditions. In hyperalkaline samples with $pH_m > \approx 11$ showing low Np solubility close to the LSC detection limit, Np concentrations were determined using a high-resolution sector field ICP-MS (Element XR, Thermo Scientific). The effective detection limit of the later including all dilution steps is about $3 \cdot 10^{-11}$ M.

1.8 Solvent extraction

The oxidation state distribution of Np in the stock solutions, in digested solid phases and in selected solubility samples (especially in the most alkaline ones with $pH_m \geq 12$ where certain contributions of Np(VI) can spontaneously form with time) were analyzed by a solvent extraction procedure using 0.5 mol·L^{-1} Di-(2-ethylhexyl) phosphoric acid (HDEHP) (p.a., Merck) in toluene (Emsure®, Merck) with and without a previous oxidation step of the sample solution with 0.08 mol·L^{-1} $K_2Cr_2O_7$ (standard reference material 136e, NIST) in 2 mol·L^{-1} HCl. The 0.5 mol·L^{-1} HDEHP extractant solution was preequilibrated with 1 mol·L^{-1} HCl before use. The basic chemicals HDEHP and toluene were stored inside the Ar box for several months before use to avoid redox artifacts from oxygen traces that may be present in the chemicals when freshly introduced to the Ar box, *c.f.*, Felmy *et al.*[6] As oxidizing agent during the solvent extraction procedure, 0.01 mol·L^{-1} $K_2Cr_2O_7$ in 1 mol·L^{-1} HCl was used. To minimize redox changes of the dissolved Np, the time between the acidification and completion of the extraction was kept as short as possible, namely about 10 minutes. The overall uncertainty of the extraction results is estimated to be about ±3%.

For the first extraction without oxidation step, an aliquot of the sample solution (typically 250 µL) was mixed with an equal volume of 2 mol·L^{-1} HCl in a 2 ml screw-capped vial (PP, Sarstedt) to make a solution with $[H^+] = 1$ mol·L^{-1}. This aqueous solution was extracted with an equal volume of the HDEHP extractant solution under intensive agitating. After phase separation by centrifugation, the organic and the aqueous phases were independently analyzed for Np by LSC. Within this procedure, initially present Np(IV)(aq) and Np(VI)(aq) is extracted into the organic phase, while Np(V)(aq), and potentially present Np(III)(aq) and undissolved Np, *i.e.*, Np(IV) particles and colloids, remain in the aqueous phase. In samples with low solubility, where the use of sector field ICP-MS was required, only the aqueous phase containing the Np(V) was analyzed. The second extraction with a previous oxidation step followed the same procedure except that the sample solution was mixed with an equal volume of the oxidation agent solution instead of the 2 mol·L^{-1} HCl. Under these conditions, $K_2Cr_2O_7$ leads to a rapid oxidation of initial Np(III)(aq) to Np(IV)(aq), and initial Np(V)(aq) to Np(VI)(aq), but leaves initial Np(IV)(aq) and Np(VI)(aq) mainly unaltered. Therefore, initially present Np(III)(aq), Np(IV)(aq), Np(V)(aq), and Np(VI)(aq) are extracted into the organic phase, whereas only Np(IV) particles and colloids remain in the aqueous phase. The extraction scheme applied is virtually the same as described by Nitsche *et al.*[7]

2. Solid phase characterization

Both Np(V) solid phases were comprehensively characterized by different analytical techniques as summarized in Table 1. The results are briefly discussed in sections 2.1 and 2.2.

Table 1: Overview of analytical techniques used for the characterization of $Na_{0.5}[NpO_2(OH)_{1.5}]\cdot 0.5H_2O$ **(I)** and $Na[NpO_2(OH)_2]$ **(II)**.

Analytical technique	**$Na_{0.5}[NpO_2(OH)_{1.5}]\cdot 0.5H_2O$**	**$Na[NpO_2(OH)_2]$**
Single crystal XRD (washed solid)	Figure 3 and Table 2	Figure 5 and Table 3
Powder XRD (washed solid)	Figure 3	Figure 5
Digital microscopy (washed solid)	Figure 1	n. a.
SEM (washed solid)	Figure 2 and Figure 4	Figure 6
EDX (washed solid)	Na : Np ≈ 0.4 : 1 and 0.46-0.52 : 1	Na : Np ≈ 1.2 : 1
ICP-OES and LSC (washed digested solid)	Na : Np ≈ 0.6 : 1	Na : Np = 0.94 : 1
Solvent extraction (washed digested solid)	≥ 96% Np(V)	≥ 96% Np(V)
Solid state Vis/NIR (washed solid)	Figure 7	Figure 7
Solubility data	Figure 8 and Table 7	Figure 8 and Table 8

2.1 $Na_{0.5}[NpO_2(OH)_{1.5}]\cdot 0.5H_2O$ (I)

Dark-violet crystals obtained within the first synthesis: the optical appearance and the observation that the material sedimented immediately and quantitatively after stirring the suspension indicated the presence of relatively large crystals. A homogeneous fraction of the washed solid phase material was placed and dried inside a screw capped quartz cuvette (Hellma, 10 mm pathlength). Digital microscopy images of this sample confirmed the presence of single crystals with well-defined platelet-like shape and maximum sizes of up to 400 micrometers, see Figure 1.

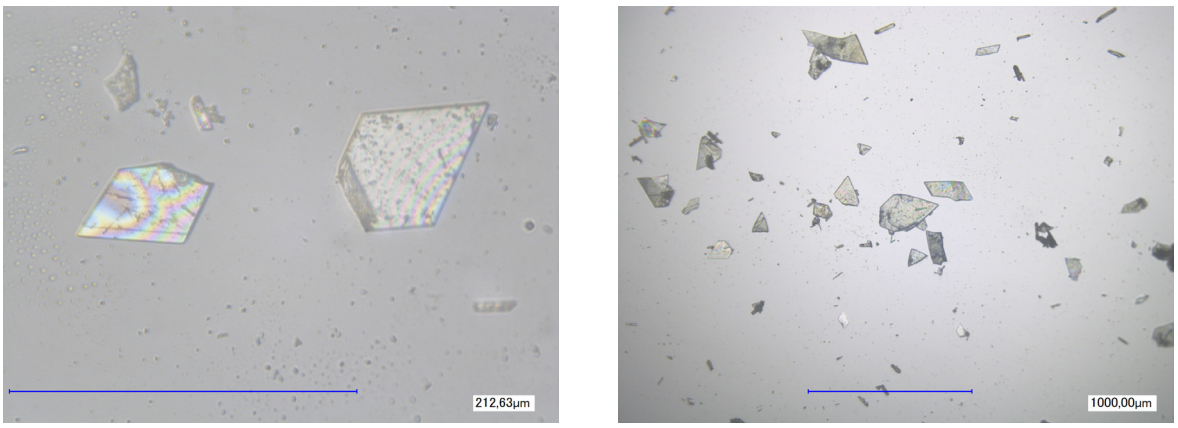

Figure 1. Digital microscope images of $Na_{0.5}[NpO_2(OH)_{1.5}]\cdot 0.5H_2O$ (I) single crystals.

A single crystal taken from the fraction in the cuvette was subsequently studied by single crystal XRD which revealed the stoichiometry $Na_{0.5}[NpO_2(OH)_{1.5}]\cdot 0.5H_2O$. The corresponding crystallographic data are summarized in Table 2. The simulated powder XRD pattern is displayed in Figure 3. Neither the stoichiometric composition nor the XRD pattern have been previously reported for a Np(V) compound.

Table 2. Crystallographic data for $Na_{0.5}[NpO_2(OH)_{1.5}]\cdot 0.5H_2O$ (I).

Empirical formula	H10 Na2 Np4 O16
Formula weight	1260.06
Temperature	183(2) K
Wavelength	0.71073 Å
Crystal system	Monoclinic
Space group	P 2_1
Unit cell dimensions	a = 5.9859(2) Å, α = 90°
	b = 10.1932(3) Å, β = 98.8640(10)°
	c = 12.1524(4) Å, γ = 90°
Volume	732.63(4) $Å^3$
Z	2
Density (calculated)	5.712 Mg/m^3
Absorption coefficient	28.270 mm^{-1}
F(000)	1064
Crystal size	0.061 x 0.058 x 0.012 mm^3
Theta range for data collection	1.696 to 38.920°.
Index ranges	$-10 \le h \le 10$, $-17 \le k \le 18$, $-21 \le l \le 21$
Reflections collected	30826
Independent reflections	8169 [R(int) = 0.0369]
Completeness to theta = 25.000°	99.9 %
Refinement method	Full-matrix least-squares on F^2
Data / restraints / parameters	8169 / 1 / 200
Goodness-of-fit on F^2	1.054
Final R indices [I > 2sigma(I)]	R1 = 0.0197, wR2 = 0.0440
R indices (all data)	R1 = 0.0205, wR2 = 0.0443
Absolute structure parameter	0.17(2)
Largest diff. peak and hole	2.042 and -2.126 $e.Å^{-3}$
CCDC/CSD no.	**2160534**

SEM analysis showed that the synthesis had dominantly led to platelet-like single crystals ranging in size from about 5 to 300 µm and, to a minor extent, to agglomerated particles consisting of smaller platelets / crystals, see Figure 2. Except the size distribution and agglomeration status, no apparent differences in the morphology between both fractions were observed. SEM-EDX further revealed that the large single crystals and the small agglomerated crystalline particles are chemically not distinguishable, both being Na-Np-O compounds with Na:Np ratio of 0.36-0.41 : 1. Considering the semi-quantitative nature of EDX results under the present setup, the obtained result is in good agreement with the Na : Np ratio in **(I)** based on the single crystal analysis. The SEM-EDX results suggest that the synthesis led to a chemically homogenous crystalline compound differing only in the crystal size.

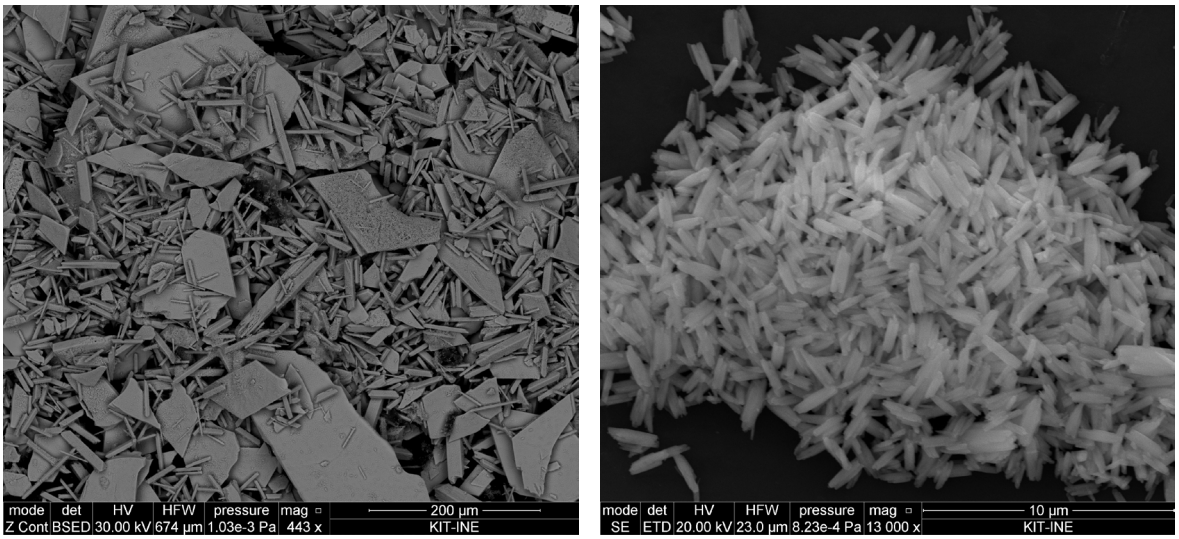

Figure 2. Scanning electron microscope images of $Na_{0.5}[NpO_2(OH)_{1.5}]\cdot 0.5H_2O$ (I). The material was dominantly present as single crystals (left; EDX analysis: ratio Na : Np = 0.41 : 1) and, to a minor extent, as polycrystalline particles (right; EDX analysis: ratio Na : Np = 0.36 : 1).

Analysis of the washed, digested solid phase by ICP-OES and LSC (quantitative chemical analysis) revealed molar ratios of Na : Np of about 0.6 : 1 which is close to the expected values for the structural Na- and Np-contents of compound **(I)**. The slightly greater Na content may be explained by potential NaOH residues from the mother liquor. On the other hand, the overall uncertainty of this approach which uses two independent analytical methods is just in the order of ±0.1.

Dark-violet crystals obtained within the second synthesis: the powder XRD pattern of that material is displayed in Figure 3. It matches very well the simulated pattern from the single crystal analysis performed with $Na_{0.5}[NpO_2(OH)_{1.5}]\cdot 0.5H_2O$ **(I)** from the initial synthesis, confirming that both synthesis routes have led to the same material.

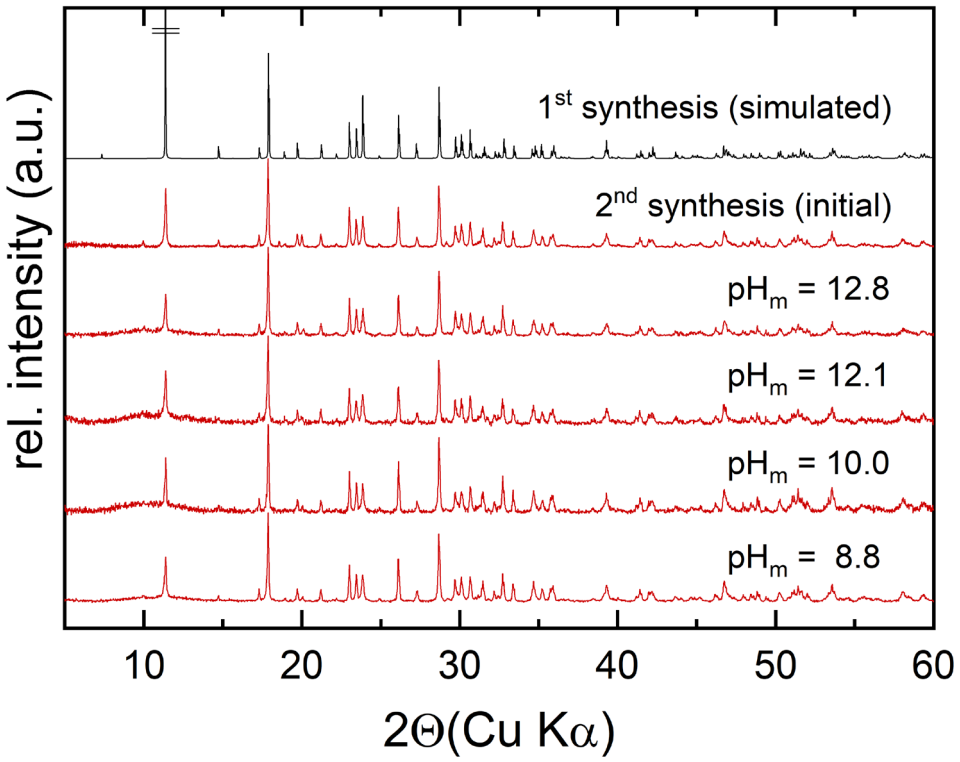

Figure 3. Powder XRD pattern of $Na_{0.5}[NpO_2(OH)_{1.5}]\cdot 0.5H_2O$ (I) used for the solubility study (initial material and the corresponding equilibrium solids retrieved from selected solubility samples with pH_m = 8.8, 10.0, 12.1 and 12.8 at the termination of the solubility study) in comparison to the simulated powder XRD pattern from the single crystal analysis.

Compound **(I)** obtained in the second synthesis was dominantly present as agglomerated crystals and, with significantly smaller contribution, as large single crystals, see SEM images in Figure 4. This is likely due to the faster cooling down phase conducted in the second synthesis compared to the initial one (3 hours versus 96 hours). Analogous to the first synthesis, SEM-EDX confirmed that both fractions (the large single crystals and the agglomerated particles) are chemically not distinguishable showing Na : Np ratios of 0.46-0.52 : 1, *i.e.*, very close to the value found for compound **(I)** in the single crystal analysis. Overall, the material was found to be chemically homogeneous.

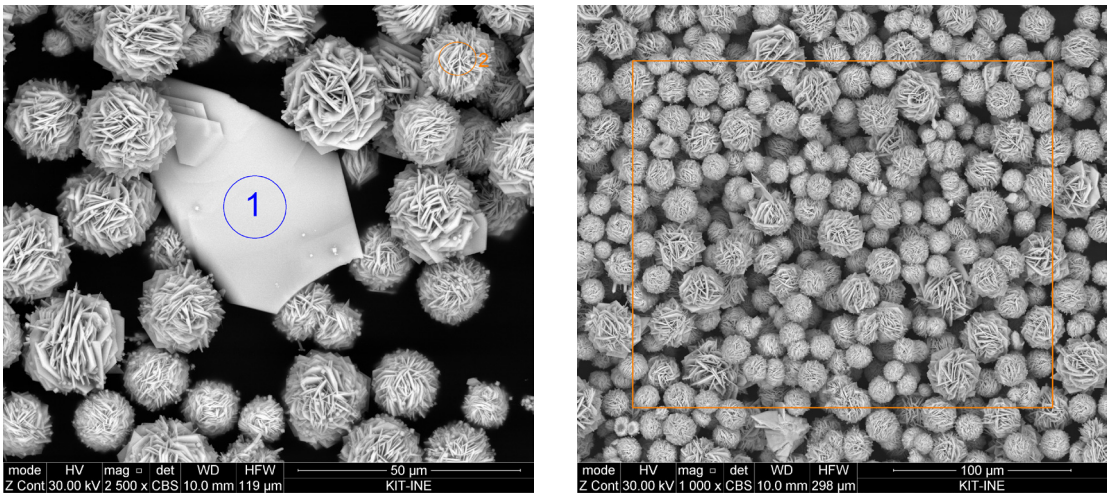

Figure 4. Scanning electron microscope images of $Na_{0.5}[NpO_2(OH)_{1.5}]\cdot 0.5H_2O$ (I). The material obtained from the second synthesis was dominantly present as agglomerated crystals (EDX analysis 1: ratio Na : Np = 0.46 : 1) and, to a minor extent, as large single crystals (EDX analysis 2: ratio Na : Np = 0.50 : 1). The overview image (right) indicates a chemically homogeneous material (EDX analysis: ratio Na : Np = 0.52 : 1).

Information about the Np oxidation state distribution in $Na_{0.5}[NpO_2(OH)_{1.5}]\cdot 0.5H_2O$ **(I)** was obtained by liquid extraction of a digested solid phase fraction. The results of the HDEHP extraction after the oxidation step with $K_2Cr_2O_7$ revealed that 99.4% of the Np were extracted with HDEHP, confirming that nearly all the Np was present as aqueous Np(aq). Without the oxidation step, only ≈3.4% of the Np (*i.e.*, Np(IV)(aq) and Np(VI)(aq)) were extracted by HDEHP, while ≈96.6% of the Np remained in the aqueous phase (*i.e.*, Np(III)(aq), Np(V)(aq) and undissolved Np). Combining the results with the fact that contributions of Np(III)(aq) did not play any role under the experimental conditions, the oxidation state of the digested solid phase is ≈96.0% Np(V)(aq). This confirms that $Na_{0.5}[NpO_2(OH)_{1.5}]\cdot 0.5H_2O$ **(I)** is a Np(V) compound.

2.2 $Na[NpO_2(OH)_2]$ (II)

A single crystal taken from a washed fraction of this material was analyzed by single crystal XRD which revealed the stoichiometry $Na[NpO_2(OH)_2]$. The corresponding crystallographic data are summarized in Table 3. The simulated powder XRD pattern is displayed in Figure 5. The stoichiometric composition and the diffraction data are in very good agreement with the ones previously reported for $Na[NpO_2(OH)_2]$ by Almond *et al.* (hydrothermal reaction of Np(V) and NaOH in an aqueous solution with a pH of 14 over 3 days at 120 °C).[8]

Table 3. Crystallographic data for $Na[NpO_2(OH)_2]$ (II).

Empirical formula	H2 Na Np O4
Formula weight	326.01
Temperature	133(2) K
Wavelength	0.71073 Å
Crystal system	Orthorhombic
Space group	$P2_12_12_1$
Unit cell dimensions	a = 5.856(7) Å, α = 90°
	b = 7.621(9) Å, β = 90°
	c = 8.174(9) Å, γ = 90°
Volume	364.8(7) $Å^3$
Z	4
Density (calculated)	5.936 Mg/m^3
Absorption coefficient	28.451 mm^{-1}
F(000)	552
Crystal size	0.050 x 0.005 x 0.005 mm^3
Theta range for data collection	3.655 to 28.766°.
Index ranges	$-7 \leq h \leq 7, -10 \leq k \leq 10, -10 \leq l \leq 10$
Reflections collected	880
Independent reflections	880
Completeness to theta = 25.000°	100.0 %
Refinement method	Full-matrix least-squares on F^2
Data / restraints / parameters	880 / 0 / 55
Goodness-of-fit on F^2	0.920
Final R indices [I > 2sigma(I)]	R1 = 0.0590, wR2 = 0.0981
R indices (all data)	R1 = 0.1113, wR2 = 0.1101
Absolute structure parameter	0.08(19)
Largest diff. peak and hole	3.267 and -2.934 $e.Å^{-3}$
CCDC/CSD no.	**2160535**

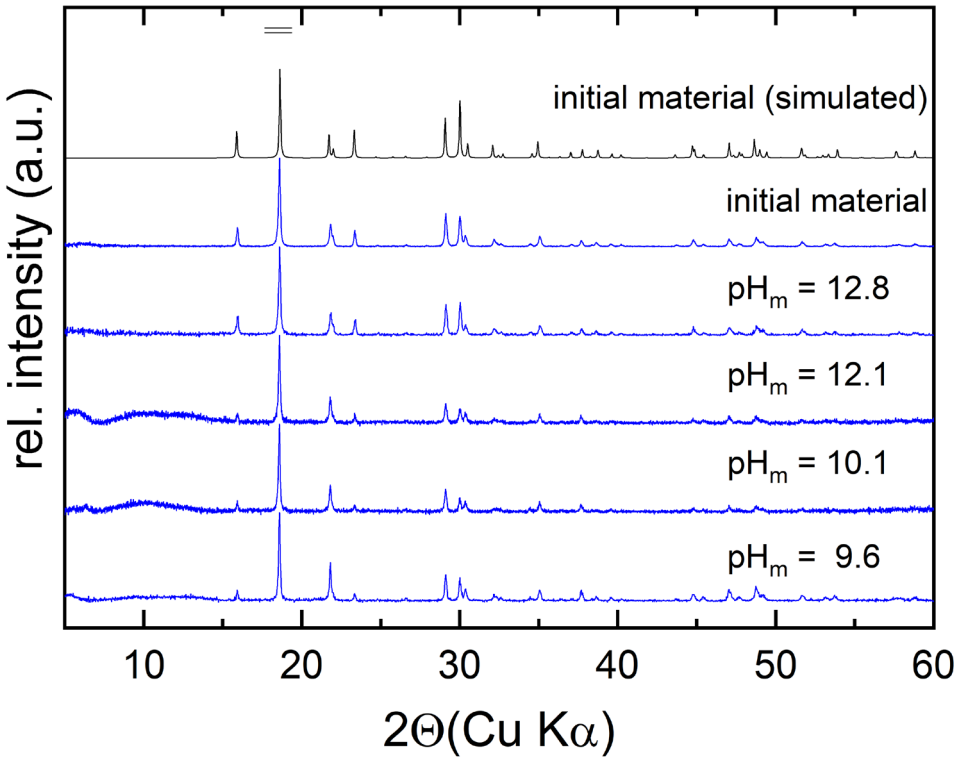

Figure 5. Powder XRD pattern of $Na[NpO_2(OH)_2]$ (II) used for the solubility study (initial material and the corresponding equilibrium solids retrieved from selected solubility samples with pH_m = 9.6, 10.1, 12.1 and 12.8 at the termination of the solubility study) in comparison to the simulated powder XRD pattern from the single crystal analysis.

SEM analysis of compound (II) showed that the synthesis had quantitatively led to thin crystalline needles of up to 100 µm length, see Figure 6. Qualitative SEM-EDX analysis confirmed the presence of structural Na and Np with a ratio of 1.2±0.2 : 1 based on nine analyses, *i.e.*, close to the expected value.

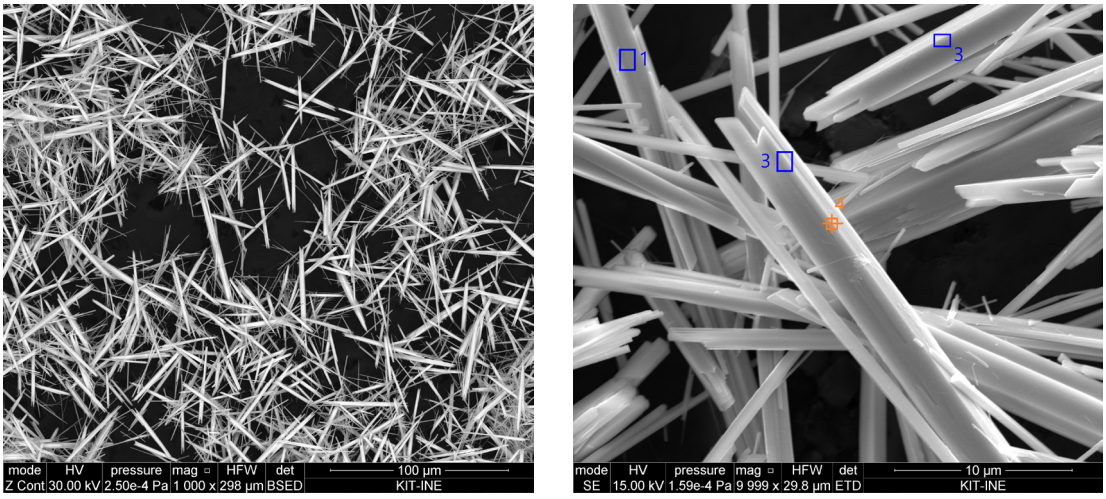

Figure 6. Scanning electron microscope images of $Na[NpO_2(OH)_2]$ (II). The material obtained in the synthesis crystalized as thin needles. Exemplary SEM-EDX analyses 1 to 4 (right) reveals ratios of Na : Np = 1.14 : 1 / 1.42 : 1 / 1.19 : 1 / 1.07 : 1.

Quantitative chemical analysis of the digested solid phase by ICP-OES and LSC revealed a molar ratio of Na : Np of 0.94 : 1 which further corroborates the stoichiometric composition of compound **(II)** based on the single crystal XRD results. 99.4% of the Np of the digested solid phase **(II)** were extracted with HDEHP after the oxidation step with $K_2Cr_2O_7$, confirming that nearly all the Np was present as aqueous Np(aq). Without the oxidation step, only ≈3.2% of the Np (*i.e.*, Np(IV)(aq) and Np(VI)(aq)) were extracted by HDEHP, while ≈96.8% of the Np remained in the aqueous phase (*i.e.*, Np(III)(aq), Np(V)(aq) and undissolved Np). As contributions of Np(III)(aq) did not play any role under the experimental conditions, and as undissolved Np was shown to be practically absent, the non-extracted ≈96% of Np corresponded to Np(V)(aq) which confirms that $Na[NpO_2(OH)_2]$ **(II)** is a pure Np(V) compound.

2.3 Solid state Vis/NIR of $Na_{0.5}[NpO_2(OH)_{1.5}]\cdot 0.5H_2O$ (I) and $Na[NpO_2(OH)_2]$ (II)

The solid state Vis/NIR absorption spectra of compounds **(I)** and **(II)** are displayed in Figure 7 in comparison to the spectrum of the $NpO_2(H_2O)_5^+$ aquo ion in 2% HNO_3 solution. The latter is characterized by its prominent NIR band at λ_{max} = 980.2 nm with $\varepsilon \approx 395$ L·mol^{-1}·cm^{-1} and FWHM ≈ 7 nm.[9,10] Analogous to solution complexes of Np(V) with ligands such as OH^-, CO_3^{2-} or carboxylates, this prominent NIR band is red-shifted and broadened in both hydroxide solid phases.[11,12,13] It is further apparent that the intensity of the less intense absorption bands of the Np(V) aquo ion are significantly enhanced in the solid phases relative to the prominent NIR band. In compound **(I)**, the prominent NIR band appears as splitted band consisting of two overlapped singlet bands of very similar intensity. These two singlet bands – Gaussian curve fitting reveals $\lambda_{max} \approx 1023$ nm with FWHM ≈ 43 nm and $\lambda_{max} \approx 1057$ nm with FWHM ≈ 42 nm, respectively – are indicative for two *distinguishable* neptunyl(V) sites in compound **(I)**. Based on the single crystal results, the structure of compound **(I)** contains four crystallographically distinct neptunium sites, Np(1) to Np(4). As discussed in the main paper, Np(1) and Np(4) have formally the same coordination environment, namely $(NpO_2)(O)_2(OH)_3$ pentagonal bipyramids[i], with only marginal differences in the crystallographic features. Likewise, Np(2) and Np(3) show formally the same coordination environments, namely $(NpO_2)O(OH)_4$ pentagonal bipyramids[i], that have again very similar crystallographic features. It is, therefore, very likely, that these two pairs of Np sites with distinguishable chemical environments just represent the two singlet contributions to the prominent NIR band. In **$Na[NpO_2(OH)_2]$ (II)**, the prominent NIR band appears as a singlet band at $\lambda \approx$ 1041 nm with FWHM ≈ 38 nm. This is in full agreement with the fact that compound **(II)** only contains one crystallographically unique neptunyl(V) sites, namely $(NpO_2)O(OH)_4$ pentagonal bipyramids[i].

[i] More precise expressions of the coordination sites are $(Np(O_{ax})(O_{ax\_2\text{-center CCI}})(O_{eq\_2\text{-center CCI}})_2(OH_{eq\_2\text{-center BL}})_2(OH_{eq\_3\text{center BL}})$ for Np(1) and Np(4) in compound **(I)**, $(Np(O_{ax\_2\text{-center CCI}})_2(O_{eq\_2\text{-center CCI}})(OH_{eq\_2\text{-center BL}})_2(OH_{eq\_3\text{center BL}})_2$ for Np(2) and Np(3) in compound **(I)**, and $(Np(O_{ax})(O_{ax\_2\text{-center CCI}})(O_{eq\_2\text{-center CCI}})(OH_{eq\_2\text{-center BL}})_4$ for Np(1) in compound **(II)**.

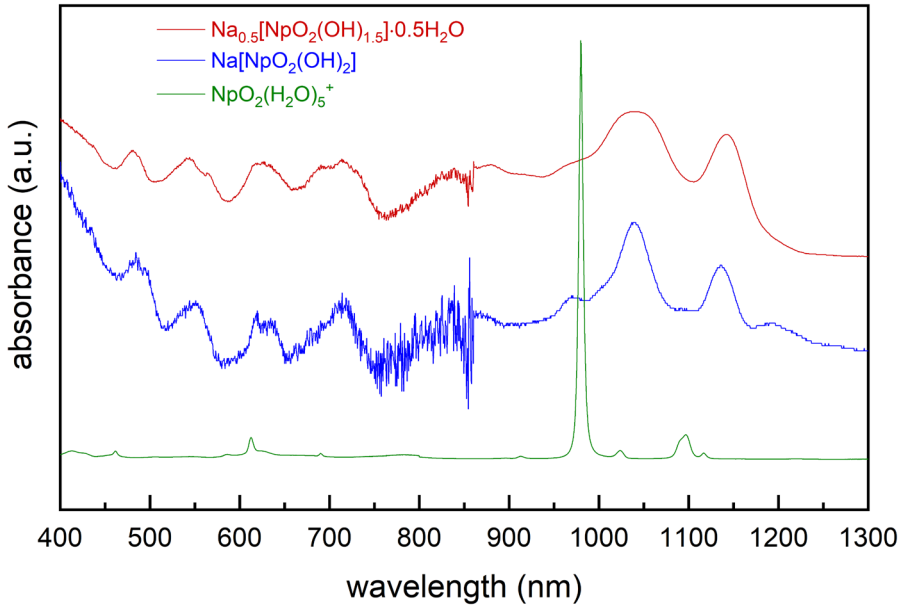

Figure 7. Solid state Vis/NIR absorption spectra of $Na_{0.5}[NpO_2(OH)_{1.5}]\cdot 0.5H_2O$ (I) and $Na[NpO_2(OH)_2]$ (II) in comparison to the one of the $NpO_2(H_2O)_5^+$ aquo ion.

3. Additional information on the solubility study and the thermodynamic evaluation

The experimentally determined solubility data for $Na_{0.5}[NpO_2(OH)_{1.5}]\cdot 0.5H_2O$ **(I)** and $Na[NpO_2(OH)_2]$ **(II)** are listed in Table 7 and Table 8 and displayed in Figure 8 together with the results of model calculations with the specific ion interaction theory (*SIT*), as outlined in the following. The fact, that no significant trend with time in log [Np(V)] was observed, indicate that the samples of both systems reached quickly a steady state. Furthermore, two results make it very likely that both Np(V) solids were indeed in a real equilibrium with the corresponding Np(V) aqueous species, namely the consistency of the two sets of log ß values acquired from the two independent solubility studies, and the reasonable slope-behavior observed in both solubility curves. Accompanying experiments from oversaturation could have further demonstrated that an equilibrium had been reached in the samples. These were, however, not performed in the present work, as the formation of crystalline Na-Np(V)-OH phases is kinetically slow at room temperature, particularly at $pH_m < 11$, and are typically accompanied by the initial formation of metastable phases like $NpO_2OH(am)$ or other Na-Np(V)-OH phases with Na:Np ≈0.2:1 to 1.6:1.[11] To overcome the challenge of slow transformation processes observed at room temperature, the crystalline Na-Np(V)-OH phases were synthesized in the present work at elevated temperature conditions, and subsequently studied at room temperature.

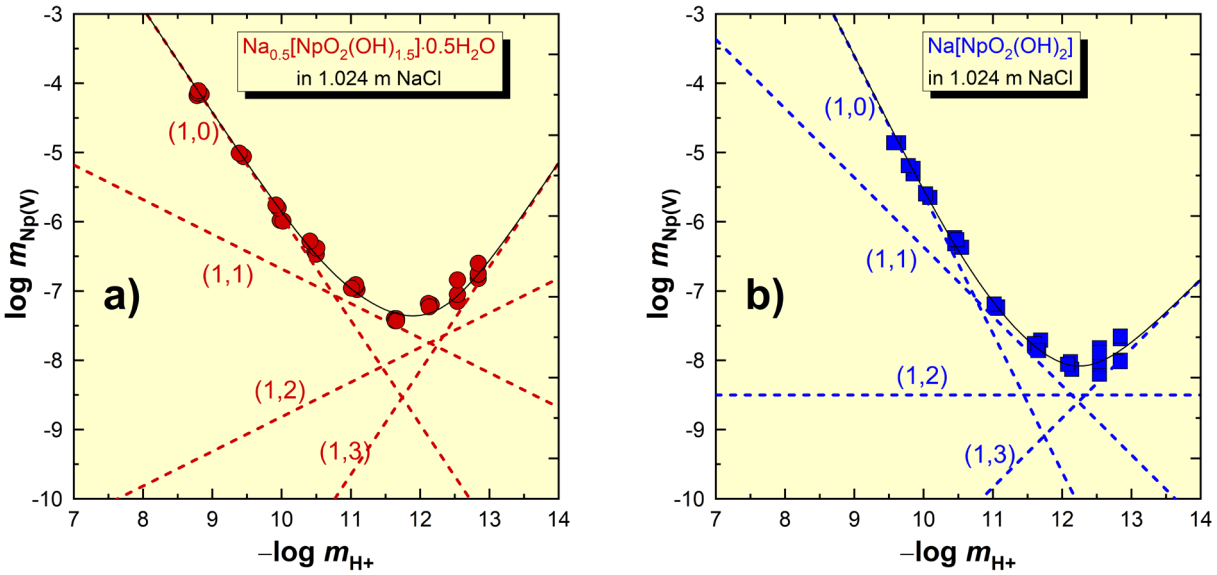

Figure 8. Experimental molal Np(V) solubility of $Na_{0.5}[NpO_2(OH)_{1.5}]\cdot 0.5H_2O$ (a) and $Na[NpO_2(OH)_2]$ (b) in 1.024 $mol\cdot kg^{-1}(H_2O)$ NaCl-NaOH solution at T = 23 ± 2ºC. Solid lines representing the overall solubility and dotted lines representing the contribution of the species NpO_2^+ (1,0), $NpO_2OH(aq)$ (1,1), $NpO_2(OH)_2^-$ (1,2) and $NpO_2(OH)_3^{2-}$ (1,3) were calculated with the *SIT* model.

The powder XRD analysis performed with solid phase fractions in selected samples at the termination of the solubility study (*c.f.*, Figure 3 and Figure 5) gave no indications for a transformation of the initially added solid phases **(I)** and **(II)**. This corroborates, that **(I)** and **(II)** were the solubility controlling solid phases in the corresponding batch series. The results of the liquid extraction performed in the supernatant solution of the solubility samples revealed that Np(V) is practically the only Np oxidation state in the aqueous phase for $pH_m \leq \sim 12.0$. However, in samples with greater pH_m, we additionally observed minor contributions of dissolved Np(VI)(aq) (about 10% at $pH_m \approx 12.5$ and 15% at $pH_m \approx 12.8$). All Np(V) solubility data shown in the graphs and tables of the present work were corrected for Np(VI) contributions.

From a thermodynamic perspective the (partial) formation of Np(VI) in the hyperalkaline Np(V) solubility samples is actually not unexpected, and can be explained by the closeness (partial overlap) of the stability fields of aqueous Np(VI) and solid Np(V). This is in particular apparent when the Pourbaix diagram for the entire Np redox state (which includes all relevant solid and aqueous Np species in the calculation) is superimposed with the Pourbaix diagram for aqueous Np species[ii], see Figure 9.

[ii] The Pourbaix diagram for aqueous Np species is calculated by neglecting contribution from Np solid phases. Still, it represents the thermodynamic stability fields of *aqueous* Np species not only in system without Np solid phases but also systems with Np solid phases.

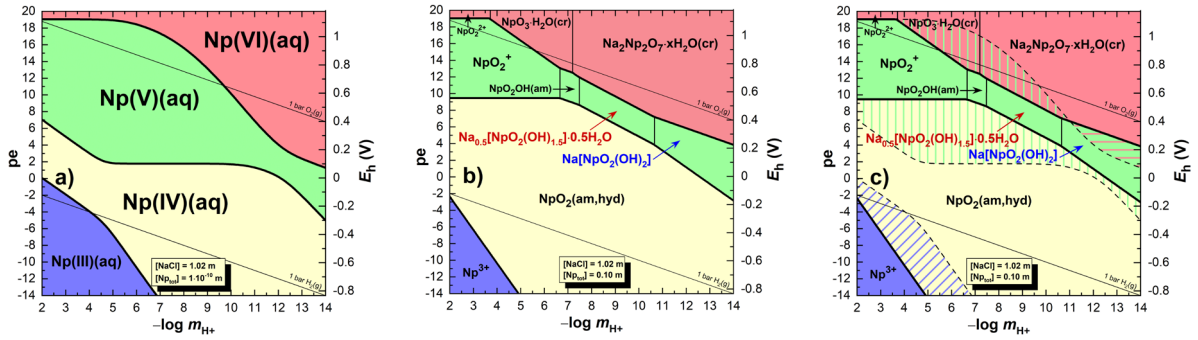

Figure 9. Pourbaix diagrams for neptunium in 1.02 mol·kg^{-1}(H_2O) NaCl. a) represents only the stability fields of aqueous Np species and b) of the entire Np system considering solid and aqueous Np species. Stability fields of a) and b) are superimposed in diagram c). Calculations were performed with thermodynamic data reported in NEA-TDB extended by the constants derived in the *p.w.*.

Figure 9 reveals that parts of the stability field of solid Np(V) fall together with the stability field of aqueous Np(VI) for $pH_m \geq 11$ (indicated as horizontal pinkish stripes). This particular area represents a pe-pH domain where solid Np(V) is the predominant Np species in the entire system, and Np(VI) is the predominant aqueous Np species. Here, the general redox equilibrium Np(V)(s) ⇔ Np(VI)(aq) controls the Np solubility. In the remaining pe-pH domains where solid Np(V) is the predominant Np species in the system, aqueous Np(V) is the prevailing aqueous Np species. Here, the "classical" solubility equilibrium, without changes in the pentavalent Np oxidation state, Np(V)(s) ⇔ Np(V)(aq) controls the Np solubility. From the experimentally determined oxidation states distribution, it is evident that the latter equilibrium was relevant for the solubility samples of the present work (which is expected for systems with an initial large inventory of Np(V) that are free of redox holding agents). However, the partial overlap, *i.e.* the closeness of the stability fields of solid Np(V) and aqueous Np(VI) can explain the formation of certain levels of Np(VI) in such hyperalkaline Np(V) systems.

As already outlined in the main paper, the shapes of the solubility curves of **(I)** and **(II)** can be explained by equilibria between the solid phases **(I)** and **(II)** and the species NpO_2^+, $NpO_2OH(aq)$, $NpO_2(OH)_2^-$ and $NpO_2(OH)_3^{2-}$. Detailed expressions of all relevant equilibrium reactions are listed in Eqs. (1) to (9). The dissolution equilibria of solids **(I)** and **(II)** with respect to the NpO_2^+ aquo ion are defined as

$$\mathbf{Na_{0.5}[NpO_2(OH)_{1.5}]\cdot 0.5H_2O + 1.5\ H^+ \Leftrightarrow 0.5\ Na^+ + NpO_2^+ + 2\ H_2O} \quad (1)$$

with

$$\log {}^*K'_{s,0} = 0.5 \log [Na^+] + \log [NpO_2^+] - 1.5 \log [H^+] \quad (1a)$$

and

$$\log {}^*K^\circ_{s,0} = \log {}^*K'_{s,0} + 0.5 \log \gamma_{Na^+} + \log \gamma_{NpO_2^+} + 2 \log a_w - 1.5 \log \gamma_{H^+} \quad (1b)$$

and

$$\mathbf{Na[NpO_2(OH)_2] + 2\ H^+ \Leftrightarrow Na^+ + NpO_2^+ + 2\ H_2O} \quad (2)$$

with

$$\log {}^*K'_{s,0} = \log [Na^+] + \log [NpO_2^+] - 2 \log [H^+] \quad (2a)$$

and

$$\log {}^*K^\circ_{s,0} = \log {}^*K'_{s,0} + \log \gamma_{Na^+} + \log \gamma_{NpO_2^+} + 2 \log a_w - 2 \log \gamma_{H^+} \quad (2b)$$

where log $*K'_{,s,0}$ and log $*K°_{s,0}$ are the conditional (valid for a given medium with $I > 0$) and the thermodynamic (valid for infinite dilution, $I = 0$) solubility constants, respectively, γi are the activity coefficients of species i, and a_w the water activity in a given medium. Eqs. (1) and (2) describe the solubility behavior of **(I)** and **(II)** reasonably well for pH_m conditions where Np(V) hydrolysis species is negligible. The latter becomes predominate at $pH_m \geq \sim 10.7$. The corresponding equilibria are defined as

$$\mathbf{NpO_2^+ + b\ H_2O \Leftrightarrow NpO_2(OH)_b^{1-b} + b\ H^+} \quad (3)$$

with

$$\log *\beta'_b = \log [NpO_2(OH)_b^{1-b}] + b \log [H^+] - \log [NpO_2^+] \quad (3a)$$

and

$$\log *\beta°_b = \log *\beta'_b + \log \gamma_{NpO_2(OH)_b^{1-b}} + b \log \gamma_{H^+} - \log \gamma_{NpO_2^+} - b \log a_w \quad (3b)$$

where log $*\beta'_b$ and log $*\beta°_b$ are the conditional (valid for a given medium with $I > 0$) and the thermodynamic (valid for infinite dilution, $I = 0$) hydrolysis constants, respectively. For a comprehensive thermodynamic description of the solubility curves of **(I)** and **(II)**, the equilibria between the solid phases and the Np(V) hydrolysis species have, therefore, to be considered as well, and can be obtained by combining Eqs. (1) and (2), respectively, with Eq. (3):

$$\mathbf{Na_{0.5}[NpO_2(OH)_{1.5}]\cdot 0.5H_2O + 0.5\ H^+ \Leftrightarrow 0.5\ Na^+ + NpO_2OH(aq) + H_2O} \quad (4)$$

with

$$\log *K'_{s,1} = \log *K'_{s,0} + \log *\beta'_1 = 0.5 \log [Na^+] + \log [NpO_2OH(aq)] - 0.5 \log [H^+] \quad (4a)$$

and

$$\log *K°_{s,1} = \log *K°_{s,0} + \log *\beta°_1 = \log *K'_{s,1} + 0.5 \log \gamma_{Na^+} + \log \gamma_{NpO_2OH(aq)} + \log a_w - 0.5 \log \gamma_{H^+} \quad (4b)$$

$$\mathbf{Na_{0.5}[NpO_2(OH)_{1.5}]\cdot 0.5H_2O \Leftrightarrow 0.5\ Na^+ + NpO_2(OH)_2^- + 0.5\ H^+} \quad (5)$$

with

$$\log *K'_{s,2} = \log *K'_{s,0} + \log *\beta'_2 = 0.5 \log [Na^+] + \log [NpO_2(OH)_2^-] + 0.5 \log [H^+] \quad (5a)$$

and

$$\log *K°_{s,2} = \log *K°_{s,0} + \log *\beta°_2 = \log *K'_{s,2} + 0.5 \log \gamma_{Na^+} + \log \gamma_{NpO_2(OH)_2^-} + 0.5 \log \gamma_{H^+} \quad (5b)$$

$$\mathbf{Na_{0.5}[NpO_2(OH)_{1.5}]\cdot 0.5H_2O + H_2O \Leftrightarrow 0.5\ Na^+ + NpO_2(OH)_3^{2-} + 1.5\ H^+} \quad (6)$$

with

$$\log *K'_{s,3} = \log *K'_{s,0} + \log *\beta'_3 = 0.5 \log [Na^+] + \log [NpO_2(OH)_3^{2-}] + 1.5 \log [H^+] \quad (6a)$$

and

$$\log *K°_{s,3} = \log *K°_{s,0} + \log *\beta°_3 = \log *K'_{s,3} + 0.5 \log \gamma_{Na^+} + \log \gamma_{NpO_2(OH)_3^{2-}} + 1.5 \log \gamma_{H^+} - \log a_w \quad (6b)$$

and

$$\mathbf{Na[NpO_2(OH)_2] + H^+ \Leftrightarrow Na^+ + NpO_2OH(aq) + H_2O} \quad (7)$$

with

$$\log *K'_{s,1} = \log *K'_{s,0} + \log *\beta'_1 = \log [Na^+] + \log [NpO_2OH(aq)] - \log [H^+] \quad (7a)$$

and

$$\log {}^*K^\circ_{s,1} = \log {}^*K^\circ_{s,0} + \log {}^*\beta^\circ_1$$
$$= \log {}^*K'_{s,1} + \log \gamma_{Na^+} + \log \gamma_{NpO_2OH(aq)} + \log a_w - \log \gamma_{H^+} \quad (7b)$$

$$\mathbf{Na[NpO_2(OH)_2] \Leftrightarrow Na^+ + NpO_2(OH)_2^-} \quad (8)$$

with

$$\log {}^*K'_{s,2} = \log {}^*K'_{s,0} + \log {}^*\beta'_2$$
$$= \log [Na^+] + \log [NpO_2(OH)_2^-] \quad (8a)$$

and

$$\log {}^*K^\circ_{s,2} = \log {}^*K^\circ_{s,0} + \log {}^*\beta^\circ_2$$
$$= \log {}^*K'_{s,2} + \log \gamma_{Na^+} + \log \gamma_{NpO_2(OH)_2^-} \quad (8b)$$

$$\mathbf{Na[NpO_2(OH)_2] + H_2O \Leftrightarrow Na^+ + NpO_2(OH)_3^{2-} + H^+} \quad (9)$$

with

$$\log {}^*K'_{s,3} = \log {}^*K'_{s,0} + \log {}^*\beta'_3$$
$$= \log [Na^+] + \log [NpO_2(OH)_3^{2-}] + \log [H^+] \quad (9a)$$

and

$$\log {}^*K^\circ_{s,3} = \log {}^*K^\circ_{s,0} + \log {}^*\beta^\circ_3$$
$$= \log {}^*K'_{s,3} + \log \gamma_{Na^+} + \log \gamma_{NpO_2(OH)_3^{2-}} + \log \gamma_{H^+} - \log a_w \quad (9b)$$

Eqs. 1 to 9 represent the principal chemical model to describe the solubility and hydrolysis behavior of solids **(I)** and **(II)** as a function of pH_m. The code *fiteql* was used to evaluate values for the conditional solubility constants log ${}^*K'_{s,0}$ for **(I)** and **(II)** and hydrolysis constants log ${}^*\beta'_n$ with n = 1,2,3 from both experimental data sets, see Table 4.[14]

Table 4. Summary of the experimental equilibrium constants in 1.02 mol·kg^{-1}(H_2O) NaCl solution independently evaluated from the solubility data for $Na_{0.5}[NpO_2(OH)_{1.5}]\cdot 0.5H_2O$ (I) and $Na[NpO_2(OH)_2]$ (II) using the model-code *fiteql* (2σ error values).[14]

constant	compound (I)	compound (II)
log ${}^*K'_{s,0}$	9.08 ± 0.03	14.40 ± 0.03
log ${}^*\beta'_1$	–10.82 ± 0.09	–10.70 ± 0.11
log ${}^*\beta'_2$	–22.85 ± 0.16	–22.93 ± 0.17
log ${}^*\beta'_3$	–35.18 ± 0.10	–35.27 ± 0.11

For the extrapolation of the conditional equilibrium constants (valid for 1.02 mol·kg^{-1}(H_2O) NaCl solution) to zero ionic strength, the *SIT* was applied in the present work.[15,16] According to the SIT, activity coefficients γ_i are defined as

$$\log \gamma_i = -z^2_i D + \Sigma\varepsilon(i,k)\, m_k$$

where z_i is the charge of the ionic species i, ε(i,k) is the ion interaction parameter between ion i and an unlike charged counterion k, m_k is the molal concentration of the counterion k, D is the Debye-Hückel term,

$$D = 0.509\sqrt{I} / (1+1.5\sqrt{I})$$

at T = 25°C with I being the molal ionic strength. The ion interaction parameters and the calculated activity coefficients valid for 1.02 mol·kg^{-1}(H_2O) NaCl solution used in the present work are

summarized in Table 5. The resulting thermodynamic equilibrium constants (valid for I = 0) are summarized in Table 6.

Table 5. SIT ion interaction parameters and calculated activity coefficients log γ_i for the species X in 1.02 mol·kg^{-1}(H_2O) NaCl used for the evaluation of the thermodynamic constants at I = 0.

species	$\varepsilon(i^+,Cl^-)$ and $\varepsilon(i^-,Na^+)$	log γ_i *(1.02 m NaCl)*	reference
Na^+	0.03 ± 0.01	−0.174 ± 0.01	NEA-TDB [16]
H^+	0.12 ± 0.01	−0.082 ± 0.01	NEA-TDB [16]
OH^-	0.04 ± 0.01	−0.164 ± 0.01	NEA-TDB [16]
NpO_2^+	0.09 ± 0.05	−0.113 ± 0.05	NEA-TDB [16]
$NpO_2OH(aq)$	0	0	NEA-TDB [16]
$NpO_2(OH)_2^-$	–0.05 ± 0.1	−0.26 ± 0.1	Hummel *et al.* (estimate) [17]
$NpO_2(OH)_3^{2-}$	–0.10 ± 0.1	−0.92 ± 0.1	Hummel *et al.* (estimate) [17]
H_2O	a_w = 0.9661		Pitzer [5]

Table 6. Summary of the thermodynamic equilibrium constants at I = 0 (2σ error values) calculated from the conditional constants using the specific ion interaction theory (*SIT*) in comparison to the current NEA-TDB selection.[16] Recommended values are highlighted in bold.

constant	compound (I)	compound (II)	mean values	NEA-TDB
log $*K°_{s,0}$	**9.06 ± 0.03**	**14.47 ± 0.03**	-	-
log $*\beta°_1$	*–10.77 ± 0.09*	*–10.65 ± 0.11*	**–10.71 ± 0.14**	–11.3 ± 0.3
log $*\beta°_2$	*–23.13 ± 0.16*	*–23.21 ± 0.17*	**–23.17 ± 0.23**	–23.6 ± 0.6
log $*\beta°_3$	*–36.19 ± 0.10*	*–36.28 ± 0.11*	**–36.23 ± 0.16**	-

Table 7. Experimental solubility data for $Na_{0.5}[NpO_2(OH)_{1.5}]\cdot 0.5H_2O$ **(I)** in 1.02 mol·kg^{-1}(H_2O) NaCl solutions.

sample	pH_m	log [Np(V)]$_m$	comment
(I)_A	8.78	−4.18	4 samplings within t_{eq} = 197 d. Powder XRD after termination.
	8.84	−4.16	
	8.79	−4.14	
	8.80	−4.11	
(I)_B	12.54	−7.05	4 samplings within t_{eq} = 22 d. pH_m calculated from analytical = initial [OH^-].
	12.54	−7.15	
	12.54	−7.05	
	12.54	−6.84	
(I)_C	11.09	−6.98	4 samplings within t_{eq} = 208 d.
	11.07	−6.93	
	11.07	−6.91	
	11.01	−6.96	
(I)_D	10.48	−6.43	4 samplings within t_{eq} = 22 d.
	10.50	−6.47	
	10.51	−6.38	
	10.41	−6.28	
(I)_E	9.98	−5.98	4 samplings within t_{eq} = 26 d. Powder XRD after termination.
	10.02	−5.99	
	9.95	−5.80	
	9.92	−5.76	
(I)_F	12.84	−6.82	4 samplings within t_{eq} = 22 d. pH_m calculated from analytical = initial [OH^-]. Powder XRD after termination.
	12.84	−6.76	
	12.84	−6.75	
	12.84	−6.60	
(I)_G	12.16	−7.20	4 samplings within t_{eq} = 48 d. Powder XRD after termination.
	12.12	−7.18	
	12.13	−7.23	
(I)_H	9.45	−5.06	2 samplings within t_{eq} = 14 d.
	9.39	−5.01	
(I)_I	11.63	−7.40	4 samplings within t_{eq} = 26 d.
	11.66	−7.40	
	11.64	−7.43	
	11.66	−7.43	

Table 8. Experimental solubility data for $Na[NpO_2(OH)_2]$ **(II)** in 1.02 $mol \cdot kg^{-1}(H_2O)$ NaCl solutions.

sample	pH_m	log $[Np(V)]_m$	comment
(II)_A	10.45	−6.32	4 samplings within t_{eq} = 169 d.
	10.45	−6.23	
	10.55	−6.37	
	10.48	−6.26	
(II)_B	11.07	−7.23	3 samplings within t_{eq} = 208 d.
	11.07	−7.25	
	11.02	−7.19	
(II)_C	11.69	−7.71	4 samplings within t_{eq} = 142 d.
	11.66	−7.86	
	11.60	−7.76	
	11.65	−7.86	
(II)_D	12.84	−8.00	4 samplings within t_{eq} = 142 d. pH_m calculated from analytical = initial $[OH^-]$. Powder XRD after termination.
	12.84	−8.02	
	12.84	−7.69	
	12.84	−7.65	
(II)_E	12.12	−8.02	3 samplings within t_{eq} = 48 d. Powder XRD after termination.
	12.14	−8.13	
	12.08	−8.06	
(II)_F	12.54	−8.20	5 samplings within t_{eq} = 142 d. pH_m calculated from analytical = initial $[OH^-]$.
	12.54	−8.06	
	12.54	−8.02	
	12.54	−7.82	
	12.54	−7.89	
(II)_G	10.09	−5.65	2 samplings within t_{eq} = 48 d. Powder XRD after termination.
	10.03	−5.60	
(II)_H	9.85	−5.31	3 samplings within t_{eq} = 14 d.
	9.85	−5.23	
	9.78	−5.19	
(II)_I	9.64	−4.86	2 samplings within t_{eq} = 14 d. Powder XRD after termination.
	9.57	−4.86	

4. Additional depictions of the structures of $Na_{0.5}[NpO_2(OH)_{1.5}]\cdot 0.5H_2O$ and $Na[NpO_2(OH)_2]$

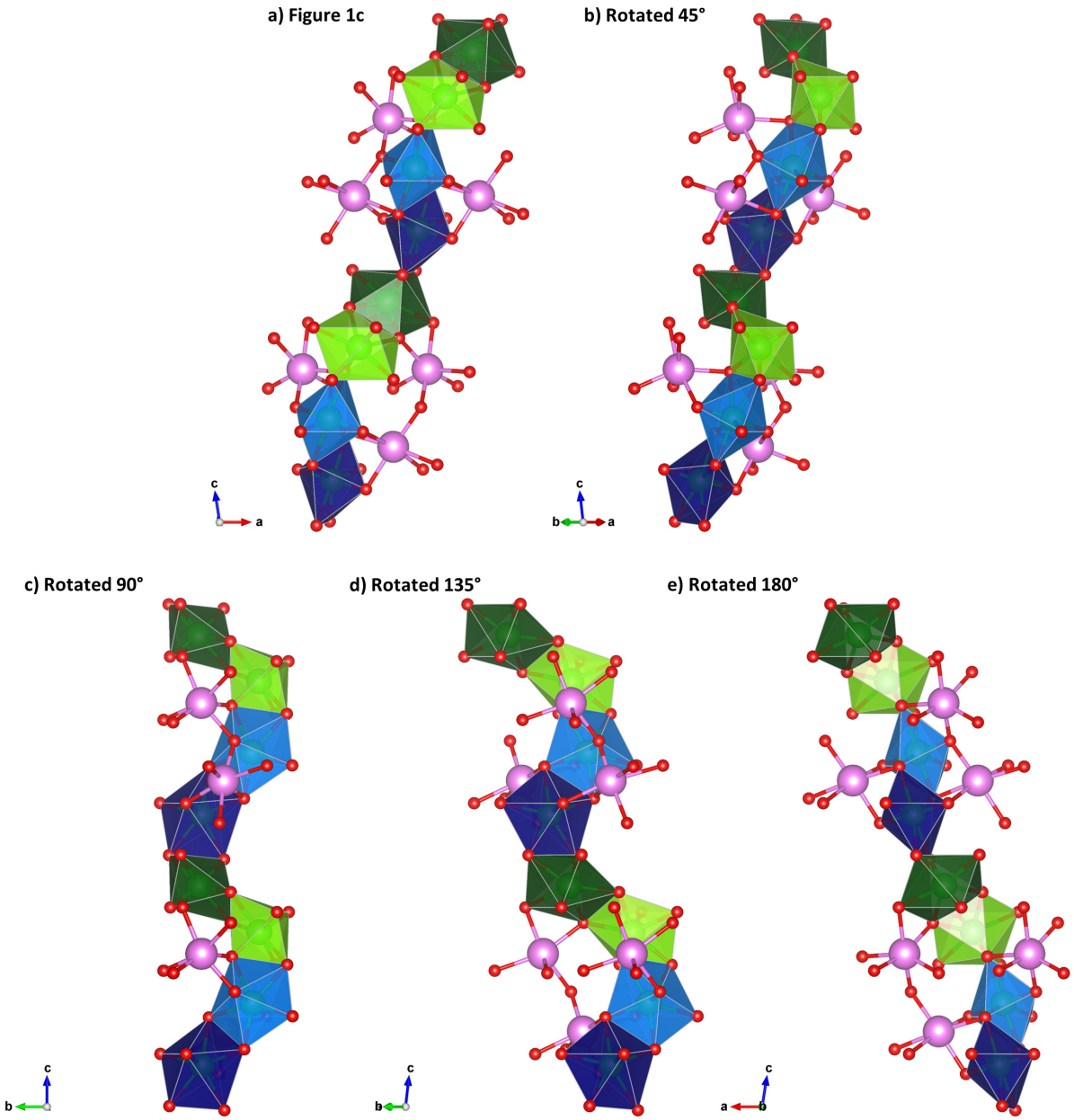

Figure 10. Additional depictions of the chain composed of $\{[Np(1)\text{-}Np(4)]\text{--}[Np(2)\text{-}Np(3)]\}_n$ dimer polymerization along the 101 plane in $Na_{0.5}[NpO_2(OH)_{1.5}]\cdot 0.5H_2O$ (I), *c.f.* Figure 1 of the main paper.[18] (Na, pink; Np(1), dark blue; Np(2), light green; Np(3), dark green; Np(4), light blue; O, red).

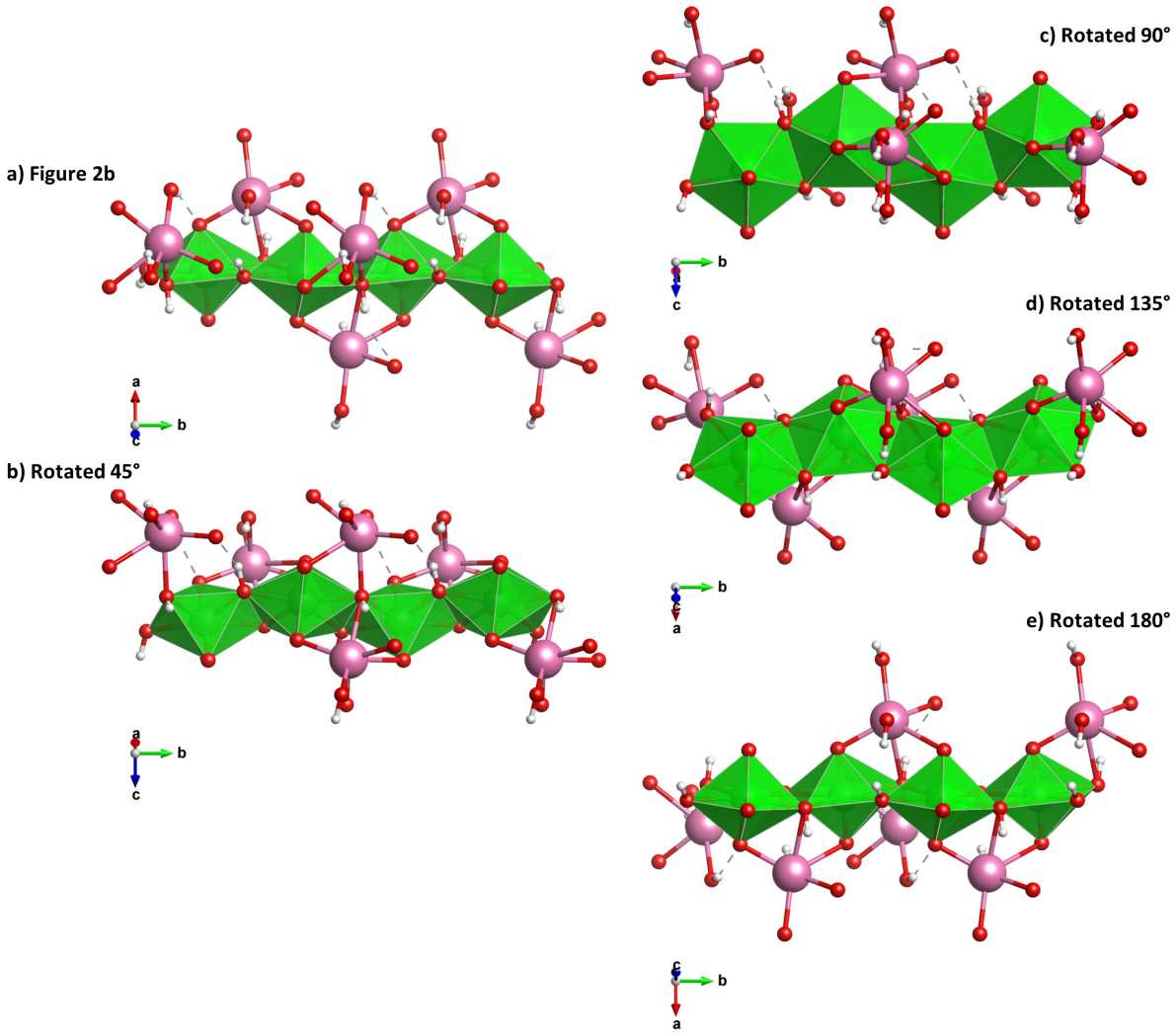

Figure 11. Additional depictions of the $(NpO_2)O(OH)_4$ pentagonal bipyramid chain in $Na[NpO_2(OH)_2]$ (II) from the side view, *c.f.* Figure 2 of the main paper.[18] (Na, pink; Np, light green; O, red; H, white).

5. References

1. ASTM International *procedure C 1285-02* 2002, 1-23.
2. *SAINT, SADABS, TWINABS;* Siemens **1997**, Analytical X-ray Instruments Inc., Karlsruhe, Germany.
3. Sheldrick,G. M. *Acta Cryst.* **2008**, *A64*, 112-122.
4. Altmaier, M.; Metz, V.; Neck, V.; Müller, R.; Fanghänel, Th. *Geochim. Cosmochim. Acta* **2003**, *67(19)*, 3595-3601.
5. Pitzer, K. S. *Activity coefficients in electrolyte solutions*, CRC Press: Boca Raton, Florida 1991.
6. Felmy, A. R.; Moore, D. A.; Rosso, K. M.; Qafoku, O.; Rai, D.; Buck, E. C.; Ilton, E. S *Environ. Sci. Technol.* **2011**, *45*, 3952-3958.
7. Nitsche, H.; Lee, S. C.; Gatti, R. C. *J. Radioanal. Nucl. Chem.* **1988**, *124*, 171-185.
8. Almond, P. M.; Skanthakumar, S.; Soderholm, L.; Burns, P. C. *Chem. Mater.* **2007**, *19*, 280-28.
9. Hagan, P. G.; Cleveland, J. M. *J. Inorg. Nucl. Chem.* **1966**, *28*, 2905-2909.
10. Fellhauer, D.; Altmaier, M.; Gaona, X.; Lützenkirchen, J.; Fanghänel, Th. *Radiochim. Acta* **2016**, *104*, 381-397.
11. Petrov, V. G.; Fellhauer, D.; Gaona, X.; Dardenne, K.; Rothe, J.; Kalmykov, S. N.; Altmaier, M. *Radiochim. Acta* **2017**, *105*, 1-20.
12. Nitsche, H.; Standifer, E. M.; Silva, R. J. *Lanthanide Actinide Res.* **1990**, *3*, 203-211.
13. Maiwald, M. M.; Skerencak-Frech, A.; Panak, P. J. *New J. Chem.* **2018**, *42*, 7796-7802.
14. Herbelin, A.L., Westall, J.C., *FITEQL, a computer program for determination of chemical equilibrium constants from experimental data*, Version 4.0, Report 99-01. Department of Chemistry, Oregon State University, Corvallis, Oregon (1999).
15. Ciavatta, L. Ann. Chim. (Rome) **1980**, *70*, 551-567.
16. Grenthe, I.; Gaona, X.; Plyasunov, A. V.; Rao, L.; Runde, W. H.; Grambow, B.; Konings, R. J. M.; Smith, A. L.; Moore, E. E. *Second Update on the Chemical Thermodynamics of Uranium, Neptunium, Plutonium, Americium and Technetium*; OECD Publications: Paris, France 2020.
17. Hummel, W., *Ionic strength corrections and estimation of SIT ion interaction coefficients*, PSI Report TM-44-09-01, Paul Scherrer Institut, Villigen (Switzerland) (2009).
18. Drawings produced with VESTA: Momma, K.; Izumi, F. VESTA 3 for Three-Dimensional Visualization of Crystal, Volumetric and Morphology Data. *J. Appl. Crystallogr.* **2011**, *44*, 1272-1276.